Effects of multiple scattering, attenuation and dispersion in waveguide sensing of fish

Mark Andrews, Zheng Gong, and Purnima Ratilal[a)]
Department of Electrical and Computer Engineering, Northeastern University, 360 Huntington Avenue, Boston, Massachusetts 02115

(Received 8 January 2010; revised 1 June 2011; accepted 29 June 2011)

An ocean acoustic waveguide remote sensing system can instantaneously image and continuously monitor fish populations distributed over continental shelf-scale regions. Here it is shown theoretically that the areal population density of fish groups can be estimated from their incoherently averaged broadband matched filtered scattered intensities measured using a waveguide remote sensing system with less than 10% error. A numerical Monte-Carlo model is developed to determine the statistical moments of the scattered returns from a fish group. It uses the parabolic equation to simulate acoustic field propagation in a random range-dependent ocean waveguide. The effects of (1) multiple scattering, (2) attenuation due to scattering, and (3) modal dispersion on fish population density imaging are examined. The model is applied to investigate population density imaging of shoaling Atlantic herring during the 2006 Gulf of Maine Experiment. Multiple scattering, attenuation and dispersion are found to be negligible at the imaging frequencies employed and for the herring densities observed. Coherent multiple scattering effects, such as resonance shifts, which can be significant for small highly dense fish groups on the order of the acoustic wavelength, are found to be negligible for the much larger groups typically imaged with a waveguide remote sensing system.
 [DOI: 10.1121/1.3614542]

PACS number(s): 43.30.Sf, 43.30.Vh, 43.30.Gv, 43.20.Fn [WLS] Pages: 1253–1271

I. INTRODUCTION

An ocean acoustic waveguide remote sensing system[1–5] can instantaneously image fish populations and continuously monitor their behaviors over continental shelf-scale regions. It utilizes the capacity of the ocean to act as a waveguide where sound can propagate long ranges via trapped modes. The imaging frequency typically employed by the system ranges from several hundred Hz to a few kHz, while its imaging diameter ranges from tens to hundreds of kilometers, determined by the source level, pulse repetition interval, and receiving array aperture.[1,3,6–8]

The waveguide remote sensing system comprises of a vertical source array that transmits broadband pulses radiated with azimuthal symmetry in the horizontal to ensonify targets of interest, and a towed horizontal hydrophone array that receives the scattered returns, as shown in Fig. 1(a). The data measured by the receiver array are beamformed to determine the azimuths of the scattered returns, and then matched filtered and charted in range. The matched filter is applied to achieve high spatial resolution in range localization and to optimize signal-to-noise ratios by exploiting the coherent gain of broadband signals with large time-bandwidth products much greater than one.[9–11]

Numerous issues must be considered when inferring the areal population densities, spatial distributions, or mean target strengths of fish populations from their matched filtered scattered intensities measured with the waveguide remote sensing system. (1) Large numbers of individuals, ranging from tens to hundreds of thousands, are often present within each resolution cell of the imaging system so that the scattered fields from the distributed group can either combine coherently or incoherently at the receiver.[12–15] (2) When large numbers of scatterers are present in a group, multiple scattering, as well as attenuation through the fish group may affect the measured scattered levels.[12,14,16–22] (3) The acoustic field propagates long ranges in an ocean waveguide through multiple paths as waveguide modes. Modal dispersion due to the slowly propagating high order modes that arrive later in time than the low order modes lead to delayed returns that affect the measured scattered levels over the range extent of the fish group. (4) The broadband transmissions undergo spreading and absorption losses over range and scintillate in both time and space due to dynamic ocean processes, such as internal and surface waves, as well as bathymetric variations.[23–25] (5) As with any active imaging system, scattered returns from fish and other targets are measured in time and then charted to range by multiplying the measurement time with a charting speed. Modal dispersion and waveguide scintillation affect the charting speed and hence the localization accuracy of targets in a waveguide.[26,27] (6) The matched filter operation is a coherent process that involves correlating the scattered field with the transmitted waveform;[10,12,28] however, the scattered returns from distributed groups are often assumed to be incoherent, and the spatial resolution from matched filtering in the *waveguide*[1–4] is assumed to be the same as that for discrete targets in free space with coherently scattered returns.

To address these issues, a numerical Monte-Carlo model is developed to determine the statistical moments of the broadband matched filtered scattered field from a three-dimensional

[a)]Author to whom correspondence should be addressed. Electronic mail: purnima@ece.neu.edu.

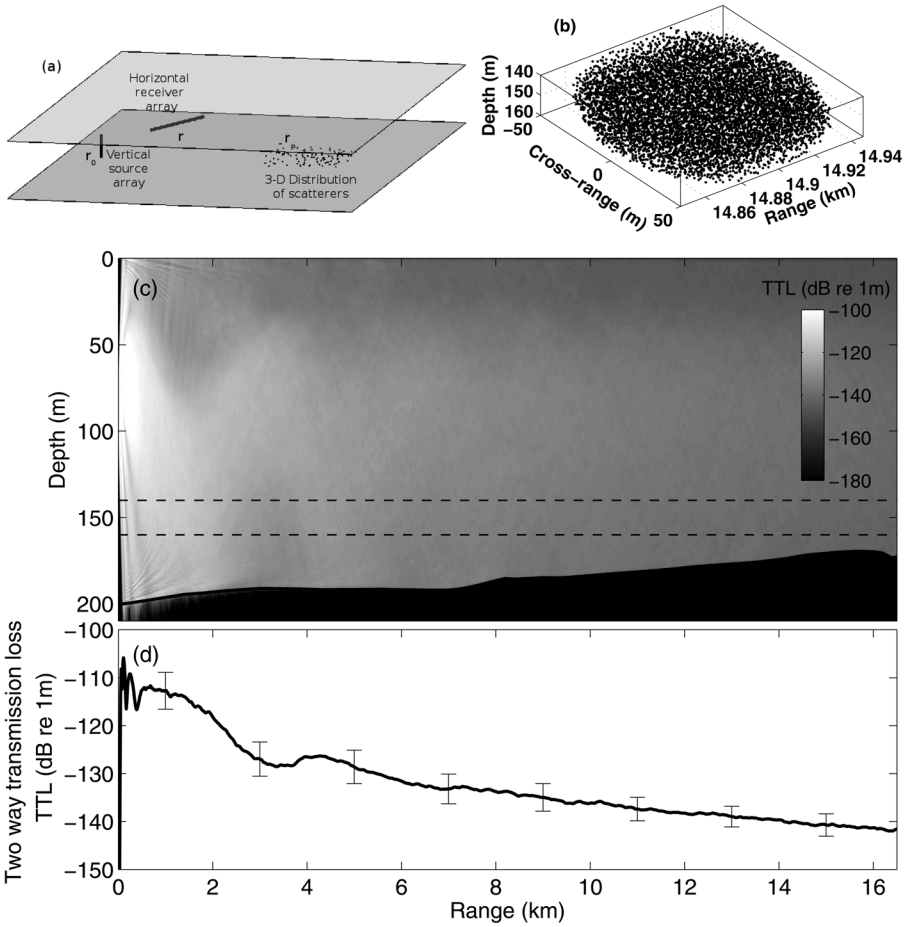

FIG. 1. (a) Geometry of the bistatic acoustic imaging system in an ocean waveguide. (b) 3D spatial configuration of a large herring group containing 7831 individuals uniformly distributed within a volume similar to an ellipsoid that has axes dimensions of $L_x = 100$ m, $L_{y1} = 125$ m, and $L_{z1} = 33.33$ m, but with cross-range and depth extents cut at ± 50 m and ± 10 m, respectively, to the center of the herring group. The plotted volume has dimensions of $L_x = 100$ m, $L_y = 100$ m, and $L_z = 20$ m. (c) Modeled broadband two-way transmission loss TTL_W calculated using Eq. (6) from a source array to potential fish locations and from the fish locations back to the receiver array center is shown as a function of fish range and depth in the Gulf of Maine environment for a source waveform of 50 Hz bandwidth centered at $f_c = 950$ Hz. (d) The TTL_W obtained by first averaging the broadband two way propagated acoustic intensities over a 20 m thick fish layer centered at $z_s = 150$ m depth and then taking the log transform following Eq. (8). The error bars indicate one standard deviation in the broadband TTL_W over the depth layer of the fish.

(3D) random spatial distribution of fish with random sizes and of random species in a random range-dependent ocean waveguide. The model includes multiple scattering from the fish group and employs the complex scatter function to account for attenuation and dispersion due to scattering from an individual fish. The model uses a range-dependent acoustic propagation model[29] based on the parabolic equation to simulate propagation in a range-dependent ocean waveguide. By incorporating randomness in the waveguide environment and the dynamic scatterer group, the model can account for statistical fluctuations typically present in the data. The model simultaneously analyzes the fully scattered field that includes multiple scattering from a fish group extended over multiple range resolution cells of the imaging system without segregating fish from individual cells, since the matched filter is applied to automatically localize the scatterers in range.

The model is applied to examine population density imaging of shoaling Atlantic herring with an ocean acoustic waveguide remote sensing system in the 2006 Gulf of Maine Experiment[1,2] (GOME06) during their fall spawning season near the northern flank of Georges Bank. It is shown theoretically that high-resolution population density imaging of fish can be achieved in the random range-dependent ocean waveguide with less than 10% error.

The numerical model developed in this paper is the only model to simultaneously analyze multiple scattering and attenuation from fish groups imaged at long ranges in an ocean waveguide with a broadband pulsed system employing the waveguide Green's function for propagation and the matched filter to localize scatterers in range. There are several useful theoretical models for analyzing and predicting the scattered levels from objects in an ocean waveguide;[30,31] however, they typically do not consider multiple scattering within the group. Previous models[12,17–20] that include multiple scattering from fish groups are restricted to direct-path imaging systems since they employ the free-space Green's function and are implemented for time harmonic signals. These models consider very small schools on the order of the acoustic wavelength with a limited number of individuals. They focus on scenarios where coherent effects in multiple scattering, such as resonance shifts and sub- and super-resonance local maxima, can be significant. Here we focus on fish groups that extend tens to thousands of times the wavelength of the waveguide imaging system, where we show that the incoherent intensity dominates the scattered returns and resonance shift effects are negligible or absent. Scattering from fish groups in a waveguide is modeled in Refs. 1, 3, and 32 for herring and in Ref. 3 for several other swimbladder bearing fish, such as Alaskan pollock, Peruvian anchovy, Argentine hake, Barents Sea capelin, and Southern blue whiting, applying the single scatter assumption and compared to seafloor reverberation.

The Monte-Carlo model developed here can also be applied to analyze detection and imaging of other groups of discrete scatterers in a waveguide where multiple scattering may be significant, such as bubble clouds, swarms of AUVs, and pods of dolphins or whales.

II. THEORY

A. Numerical Monte-Carlo model for the statistical moments of the broadband matched filtered fully scattered field from a 3D random distribution of scatterers that includes multiple scattering in a random range-dependent ocean waveguide

Here, we describe the numerical Monte-Carlo model used to simulate the statistical moments of the broadband matched filtered fully scattered field that includes multiple scattering from a 3D random spatial distribution of random scatterers in a random range-dependent ocean waveguide. The model can be applied to calculate the total scattered field from a group of scatterers in any direction in a waveguide including the forward. The theoretical formulation in Appendix A follows the approach of Ref. 12 but is implemented here for a random range-dependent ocean waveguide by employing the waveguide Green's function. Model verification is provided in Sec. II C.

Consider the general bistatic geometry for the problem illustrated in Fig. 1(a), where the origin of the coordinate system is placed at the air-water interface with the positive z axis pointing downward. A vertical source array centered at $\mathbf{r}_0 = (x_0, y_0, z_0)$ and a horizontal receiver array centered at $\mathbf{r} = (0, 0, z)$ are used to image a group of scatterers centered at $\mathbf{r}_C = (x_C, y_C, z_C)$ in the far-field of both the source and receiver arrays. The group is distributed over a three dimensional volume where each pth scatterer is located at $\mathbf{r}_p = (x_p, y_p, z_p) = (\rho_p, \phi_p, z_p)$, where $\rho_p^2 = x_p^2 + y_p^2$. The source transmits waveform $q(t)$ with Fourier transform $Q(f)$ and bandwidth B.

For a specific realization of the ocean environment and scatterer group, the time-dependent broadband matched filtered fully scattered field $\Psi_s(t_M)$ that includes multiple scattering is calculated using Eq. (A6). By randomizing both the waveguide Green's function and spatial distribution of scatterers according to known statistical properties, many independent realizations of the scattered field are generated. The statistically coherent and incoherent scattered intensities from the scatterer group are then obtained from the sample squared mean $|\langle \Psi_s(t_M) \rangle|^2$ and sample variance Var $[\Psi_s(t_M)]$, respectively. The waveguide is randomized by incorporating linear internal waves along the range-dependent acoustic propagation paths from source to scatterer locations and from scatterer locations to the receiver as outlined in Sec. III A. The scatterer group is randomized through both the scatter functions and spatial locations of individuals in the group.

The acoustic field scattered from one scatterer to another, as formulated in Eq. (A4), can be solved using either matrix inversion or an iterative approach.[12] The matrix inversion approach requires an N^2 size matrix to be inverted, which makes this approach computationally cumbersome for large groups[12,18] of scatterers. In Sec. IV, we apply the iterative approach, with each iteration simulating an increasingly higher order of scattering. Computational constraints limit the number of scatterers that can be simulated in a reasonable amount of time. The multiply scattered returns from a maximum of 40 000 individuals are simulated, producing 1.6×10^9 multiple scattering interactions for each iteration of scattering.

B. Modeling the complex scatter function distribution and 3D spatial distribution for a group of fish

At frequencies ranging from a few hundred Hz to several kHz, the air-filled swimbladders of most swimbladder-bearing fish are the primary source of scattering. A fish swimbladder is modeled here as a damped air-filled prolate spheroid, as discussed in Appendix B. Fish swimbladders are acoustically compact at the operating frequencies of a typical waveguide remote sensing system because they are much smaller than the acoustic wavelength so that the scattered field from each individual fish is radially symmetric. Given a fish of known swimbladder volume, its complex scatter function is calculated using Eq. (B1).

To model the complex scatter function distribution for fish in a group distributed over a given water depth, we first assume the fish fork length L follows a Gaussian distribution with a mean and standard deviation obtained from available *in situ* trawl sample measurements.[1] The distribution of fish body volume is next calculated from the fork length distribution by applying the empirically determined non-linear weight-length regression, Eq. (B5). By assuming fish in the group are neutrally buoyant at the same depth, and fish swimbladder volume typically comprises roughly 4%–5% of fish body volume when they are neutrally buoyant, the swimbladder volume for each individual fish at any depth z can be calculated by assuming Boyle's law, as discussed in Appendix B. The distribution of complex scatter functions for fish in the group is then obtained from their swimbladder volume distribution via Eq. (B1).

To approximate the 3D spatial configurations fish groups adopt when they form either large shoals or small dense schools, we consider two models in the examples shown in Sec. II C and Sec. IV. In the first model, we assume a fully random 3D spatial configuration for fish in a group specified by its volumetric density n_V, which is a function of range, depth and cross-range. In the second model,[17,20] the fish locations in a group are only partially random and their 3D spatial configuration is derived from a basic cubic cellular unit. In this model, each fish is first arranged to be in the center of a cubic cellular unit with all closest neighbors spaced a mean distance d determined by the volumetric density,

$$d = \left(\frac{1}{n_V}\right)^{1/3}. \tag{1}$$

As fish swim, the distances between these closest neighbors will vary from the mean value d over time. To account for this variation, individual fish locations are next randomly varied from their mean positions according to a Gaussian distribution with a standard deviation σ_d assumed to be 30% of the mean inter-fish distance d. In both models, the fish areal density n_A at a given horizontal range is obtained by integrating the volumetric densities n_V over the depth distribution of the fish layer at that range.

C. Model verification

Here, the model developed in Sec. II A and Appendix A is verified by comparison with examples provided in Refs. 18 and 20 where the time-harmonic scattered intensities that include multiple scattering are calculated for a small group of fish containing 13 individuals at frequencies ranging from tens of Hz to 5 kHz, imaged by a monostatic direct-path system in an iso-speed lossless non-random environment, where the free-space Green's function is valid. All fish are identical with 40 cm total length and equivalent spherical swimbladder radius $a=2$ cm. The school is centered at $z=50$ m depth, and all fish are assumed to be neutrally buoyant at 50 m depth.

The time-harmonic fully scattered field $\Phi_s(\mathbf{r}, f)$ at frequency f that includes multiple scattering for each realization of the fish group is calculated using Eqs. (A1) to (A4) where $\mathcal{B}(\phi_p)=1$ for all fish in the group. The statistically coherent and incoherent fully scattered intensities at frequency f that include multiple scattering are obtained from the sample squared mean $|\langle\Phi_s(\mathbf{r},f)\rangle|^2$ and sample variance $\mathrm{Var}[\Phi_s(\mathbf{r},f)]$, respectively, derived from 10 independent Monte-Carlo simulations. The total scattered intensity is the sum of the two,[12] $\left\langle|\Phi_s(\mathbf{r},f)|^2\right\rangle = |\langle\Phi_s(\mathbf{r},f)\rangle|^2+\mathrm{Var}[\Phi_s(\mathbf{r},f)]$.

The coherent, incoherent and total *school* target strengths denoted by $TS_{\mathrm{coh},s}(f)$, $TS_{\mathrm{incoh},s}(f)$, and $TS_{\mathrm{tot},s}(f)$, respectively, are calculated using

$$TS_{\mathrm{coh},s}(f) = 10\log_{10}\left(|\langle\Phi_s(\mathbf{r},f)\rangle|^2\right) - SL(f) + TTL_{FS}(\mathbf{r}_s,f|\mathbf{r}_0,\mathbf{r}), \quad (2)$$

$$TS_{\mathrm{incoh},s}(f) = 10\log_{10}\{\mathrm{Var}[\Phi_s(\mathbf{r},f)]\} - SL(f) + TTL_{FS}(\mathbf{r}_s,f|\mathbf{r}_0,\mathbf{r}), \quad (3)$$

$$TS_{\mathrm{tot},s}(f) = 10\log_{10}\left(\left\langle|\Phi_s(\mathbf{r},f)|^2\right\rangle\right) - SL(f) + TTL_{FS}(\mathbf{r}_s,f|\mathbf{r}_0,\mathbf{r}), \quad (4)$$

where $SL(f)$ is the source level at frequency f, and $TTL_{FS}(\mathbf{r}_s,f|\mathbf{r}_0,\mathbf{r}) = 10\log_{10}\left(1/|\mathbf{r}_s-\mathbf{r}_0|^2\right)+10\log_{10}\left(1/|\mathbf{r}-\mathbf{r}_s|^2\right)$ is the free-space two-way transmission loss from the source to the school center $\mathbf{r}_s$ and from the school center to the receiver, respectively.

The fish are distributed in a 3D volume following the partially random lattice configuration described in Sec. II B of this article and also in Ref. 20. Each fish position is randomized with a standard deviation of $\sigma=4$ cm about the mean inter-fish spacing d set to be (a) one fish body length, $d=40$ cm, (b) quarter fish body length, $d=10$ cm, and (c) four times the fish body length, $d=1.6$ m, respectively, in Fig. 2. The coherent, incoherent and total *school* target strength spectra are compared to the estimated $TS_{\mathrm{est},s}(f)$ spectrum obtained from

$$TS_{\mathrm{est},s}(f) = TS(f) + 10\log_{10}N, \quad (5)$$

which assumes single scattering is valid, where $TS(f) = 10\log_{10}\langle|S(f)/k|^2\rangle$ is the target strength of a single fish. Here, the azimuthal angle of ensonification is kept constant and the school target strengths are estimated from backscattered intensities. This differs from the examples shown in Fig. 4 of Ref. 20, where the azimuthal angle of ensonification was randomly varied between 0 and 360 degree for each realization.

The school target strength spectra plotted in Fig. 2 are consistent with those shown in Ref. 20. At the mean inter-fish spacing of one body length [Fig. 2(a)], the resonance frequency of the school is lower than the single fish resonance frequency. The scattering is dominated by the coherent intensity near resonance, while the incoherent intensity becomes important above 1 kHz. When the mean inter-fish spacing is reduced to a quarter body length [Fig. 2(b)], the school resonance frequency shifts to a frequency much lower than that of the single fish, consistent with the findings in Fig. 8 of Ref. 18. The scattering is dominated by the coherent intensity for the most part below 5 kHz. When the mean inter-fish spacing is increased to four times the fish body length [Fig. 2(c)], there is negligible shift in the school resonance frequency compared with that of the single fish. A noticeable sub-resonance local maxima appears at about 100 Hz, and many more local maxima appear at frequencies above resonance. In general, the model developed here reproduces the key features and results reported in Refs. 17, 18, and 20. The slight differences in the school target strength local maxima at frequencies above resonance is mainly due to the fact that the azimuthal ensonification angle was not varied across the realizations here.

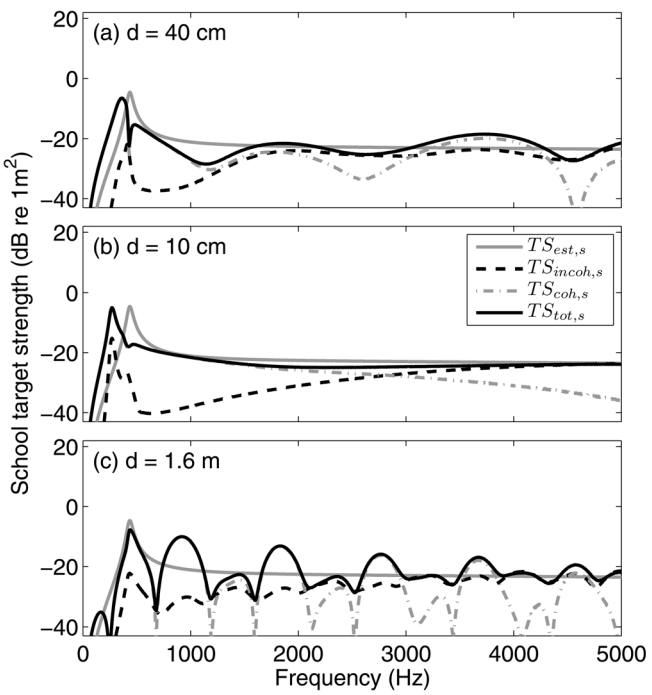

FIG. 2. Effect of varying inter-fish spacing on the *school* target strength spectra for a small fish group containing 13 individuals. The mean inter-fish spacings are (a) one fish body length, $d=40$ cm, (b) quarter fish body length, $d=10$ cm, and (c) 4 times the fish body length, $d=1.6$ m. The coherent, incoherent, total and estimated *school* target strength spectra are calculated via Eqs. (2)–(5), respectively.

III. MODELING THE 2006 GULF OF MAINE EXPERIMENT

During GOME06,[1,2] an ocean acoustic waveguide remote sensing system was employed to image and study the abundance and diurnal behavior of shoaling Atlantic herring populations during their autumn spawning season along the northern flank of Georges Bank over a 2 week period. The 100 km imaging diameter of the waveguide remote sensing system for a measurement time period of roughly 75 s enabled both massive herring shoals extending tens of kilometers and estimated to contain hundreds of millions of individuals, as well as smaller groups extending roughly 50 to 200 m and comprising fewer than 1×10^6 fish to be instantaneously imaged. The images were updated every 75 s to provide continuous monitoring of fish activity for many hours each day. Simultaneous measurements made using an ultrasonic conventional fish-finding sonar provided the local volumetric densities and depth dependence of the fish distributions.[1,2] Detailed descriptions of the experimental setup, data analysis, and results showing wide-area population density images of herring shoals are provided in Refs. 1 and 2, along with supporting oceanographic, biological, and environmental information.

Instantaneous wide-area images of the ocean environment were formed from broadband linear frequency modulated transmissions of $\tau = 1$ s duration and $B = 50$ Hz bandwidth with varying center frequencies in the 300 to 1200 Hz range. The time-bandwidth product of the signals transmitted was $\tau B = 50 \gg 1$ so that the matched filter or pulse compression[9–11] could be employed to reduce the horizontal range resolution from $\Delta\rho = c_{\text{chart}}\tau/2 = 750\,\text{m}$ to $\Delta\rho = c_{\text{chart}}/2B \approx 15\,\text{m}$, a factor of 50 improvement. The resulting 15 m horizontal range resolution of the waveguide remote sensing system is comparable to the horizontal imaging diameter of the conventional ultrasonic fisheries echosounder of roughly 20 m at 200 m water depth. The waveguide system's angular resolution $\beta(\phi_p)$ at azimuthal angle ϕ_p depend on the center frequency and array aperture used for beamforming (see Table I in Ref. 1). Its resolution footprint is dependent on both range and bearing from the receiving array, given by $A_{\text{res}}(\boldsymbol{\rho}_p) = \rho_p \Delta\rho \beta(\phi_p)$.

Incoherent averaging over 3 to 5 consecutive instantaneous wide-area images at a given frequency band was used to reduce the standard deviations and minimize the effects of noise in the images.[1,2] A single scattering assumption was employed to infer fish areal population density from the averaged scattered intensity level at a given resolution cell, after correcting for source level, a two-way transmission loss term obtained by averaging the expected waveguide Green's function over the depth extent of the fish layer, the resolution footprint of the imaging system, and the low frequency target strength obtained from the mean scattering cross section of a herring individual. The latter was estimated at each imaging frequency band by local calibration with simultaneous measurements from a conventional fish-finding sonar.[1]

Here, we implement the rigorous theoretical model described in Sec. II to prove the assumptions and approaches employed in Refs. 1–3 for inferring herring areal population densities and abundances from wide-area scattered intensity images acquired with the waveguide remote sensing system. The assumptions include (1) the incoherent intensity dominated the scattered returns from the fish group, (2) single scattering assumption is valid, (3) negligible attenuation and dispersion in the incident field from forward propagation through the fish group, (4) multi-modal waveguide dispersion is negligible in the scattered field from the fish group, (5) the minimum mean water column sound speed is used as an optimal sound speed to chart the scattered field measured as a function of time to range, and (6) negligible degradation in the range resolution and in the scattered intensity level after matched filtering with the source waveform in the ocean waveguide.

A. Modeling acoustic propagation in the random range-dependent Gulf of Maine environment

Long-range broadband acoustic propagation through a random range-dependent ocean waveguide is calculated using the parabolic equation based range-dependent acoustic propagation model, RAM.[29] This waveguide propagation model takes into account the environmental parameters, such as the range-dependent bathymetry, seafloor geo-acoustic properties, the dynamic water-column sound speed profiles, and the locations and depths of the source and receiver arrays. It provides the complex waveguide Green's function G_W, calculated at discrete frequencies over the signal bandwidth as a function of range and depth.

The acoustic fields propagated from the source array to the fish locations and from the fish locations to the receiver array center in Eqs. (A2) and (A4) are calculated separately. For the source array, the model coherently sums the acoustic fields from each element of the array for the field incident on the fish group. The source array of the waveguide remote sensing system has the effect of beaming the acoustic intensity preferentially into the low order modes of the ocean waveguide which can propagate long ranges with less attenuation than the high order modes.

Following the approach of Ref. 24, linear internal waves are simulated in the waveguide propagation model by updating the water-column sound speed profile every 500 m in range corresponding to the correlation length scale of internal waves in continental shelf environments.[25,33] The profiles are randomly selected from over 200 experimentally measured sound speed profiles acquired during the course of GOME06, shown in Fig. 3 of Ref. 1. This approach simulates the effect of internal waves in randomizing the acoustic field in the waveguide.

As an example, the broadband two-way transmission loss (*TTL*) in the range-dependent Gulf of Maine environment simulated stochastically with the waveguide propagation model is illustrated in Fig. 1(c). The TTL_W at each potential fish location $\mathbf{r}_p$ is calculated using

$$TTL_W(\mathbf{r}_p, f_c|\mathbf{r}_0, \mathbf{r}) = 10\log_{10}\left\langle (4\pi)^2 \frac{1}{E_0}\int_{f_c-B/2}^{f_c+B/2} |Q(f)|^2 \times |G_{W,s}(\mathbf{r}_p|\mathbf{r}_0, f)|^2 |G_{W,r}(\mathbf{r}|\mathbf{r}_p, f)|^2 df \right\rangle, \quad (6)$$

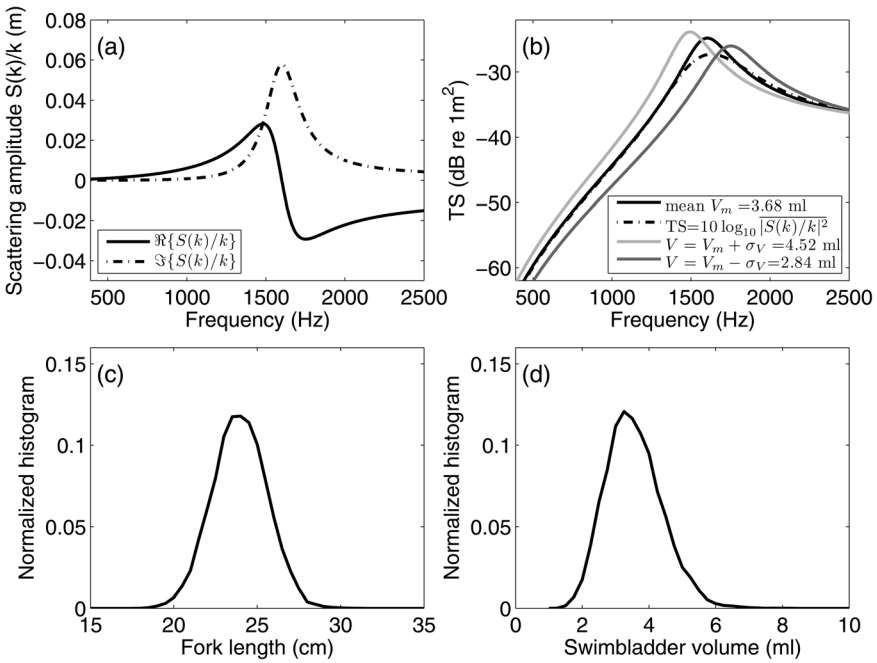

FIG. 3. (a) The real and imaginary parts of the complex scattering amplitude $S(k)/k$ for a herring of mean swimbladder volume 3.68 ml. (b) The target strengths of fish with mean swimbladdder volume (black) and of fish with swimbladder volumes both 1 standard deviation larger (light gray) and smaller (dark gray) than the mean. The ensemble-averaged target strength (dash-dotted black), $TS = 10\log_{10}|S_P(k)/k|^2$, obtained by averaging over the scattering cross-sections of all fish in the group is also plotted. The normalized histograms (by total number of fish N = 10 000) of (c) the fork length and (d) swimbladder volume for the herring group. The swimbladder volume shown in (d) is inferred from (c) and taking into account the depth of each individual fish in the group given a known neutral buoyancy depth at 85 m using Eq. (B5) and (B6), where $p = 3.35\times10^{-6}$ and $q = 3.35$ are empirically determined from length and weight measurements of trawl samples (Ref. 1).

where $G_{W,s}(\mathbf{r}_p|\mathbf{r}_0,f)$ is the *waveguide* Green's function describing the acoustic field propagation from the 10-element source array centered at $\mathbf{r}_0$ to a potential fish location $\mathbf{r}_p$, and $G_{W,r}(\mathbf{r}|\mathbf{r}_p,f)$ is the *waveguide* Green's function from that fish location to the receiver array center $\mathbf{r}$, and $E_0 = \int |Q(f)|^2 df$ is the source energy. In Fig. 1(c), the source array is centered at 65 m depth with 0.83 m spacing between the elements, transmitting a 50 Hz bandwidth Tukey windowed signal with center frequency of 950 Hz. The horizontal coordinate of the receiving array is co-located with the source, but its depth is located at $z_r = 105$ m. The propagation path is a transect from Fig. 2(a) of Ref. 1 with coordinates (0,0) to (0.5,−15) km in eastings and northings, beginning at the horizontal location of the source array and extending through a region containing a large fish shoal. The varying bathymetry along the path is plotted in black in Fig. 1(c), illustrating the gradual upslope from Georges basin to the edge of the bank. Note that the TTL_W is determined by first averaging 100 independent Monte-Carlo realizations of the source spectrum-weighted square-magnitude Green's function through the fluctuating ocean and then applying the log transform. Single realizations of the transmission loss exhibit spatial fluctuations due to modal interference. By averaging the scintillating acoustic intensities in both time and space in the dynamic ocean environment, the fluctuations in transmission loss are reduced.[24] The seafloor at the GOME06 site is mostly sandy,[34] modeled here with geo-acoustic parameters of sound speed 1700 m/s, density 1.9 g/cm^3, and attenuation 0.8 dB/wavelength. The examples in the following sections simulate the bistatic imaging of herring groups located within the main lobe of the receiver array beamed along the path indicated in Fig. 1(c).

For fish distributed over a $D = 20$ m depth layer centered at $z_s = 150$ m depth in the waveguide, Fig. 1(d) shows the TTL_W obtained by first averaging the broadband two way propagated acoustic intensities in Fig. 1(c) over the depth layer of the fish, and then taking the log transform, described by

$$TTL_W(\boldsymbol{\rho}_p, z_s, f_c|\mathbf{r}_0, \mathbf{r}) = 10\log_{10}\left\{(4\pi)^2\frac{1}{E_0}\int_{z_s-D/2}^{z_s+D/2}\left\langle\int_{f_c-B/2}^{f_c+B/2}|Q(f)|^2 \times |G_{W,s}(\boldsymbol{\rho}_p, z_p|\mathbf{r}_0,f)|^2|G_{W,r}(\mathbf{r}|\boldsymbol{\rho}_p, z_p,f)|^2 \times P(\boldsymbol{\rho}_p, z_p)df\right\rangle dz_p\right\}. \quad (7)$$

where, $P(\boldsymbol{\rho}_p, z_p)$ is the probability of finding a fish at location $(\boldsymbol{\rho}_p, z_p)$. For a uniform distribution of fish, $P(\boldsymbol{\rho}_p, z_p) = 1/D(\boldsymbol{\rho}_p)$, where $D(\boldsymbol{\rho}_p)$ is the layer depth of the fish group at horizontal location $\boldsymbol{\rho}_p$, so that

$$TTL_W(\boldsymbol{\rho}_p, z_s, f_c|\mathbf{r}_0, \mathbf{r}) = 10\log_{10}\left\{(4\pi)^2\frac{1}{E_0}\frac{1}{D(\boldsymbol{\rho}_p)}\int_{z_s-D/2}^{z_s+D/2}\left\langle\int_{f_c-B/2}^{f_c+B/2}|Q(f)|^2 \times |G_{W,s}(\boldsymbol{\rho}_p, z_p|\mathbf{r}_0,f)|^2|G_{W,r}(\mathbf{r}|\boldsymbol{\rho}_p, z_p,f)|^2 df\right\rangle dz_p\right\}. \quad (8)$$

The standard deviation in the broadband TTL_W over the depth layer of the fish at ranges greater than 10 km is roughly 2 to 3 dB, as shown in Fig. 1(d), indicating the two-way propagated broadband acoustic field is only partially randomized.

The *inter-fish* acoustic propagation in Eq. (A4) is approximated by the free space Green's function, G_{FS},

$$G_{FS}(\mathbf{r}_n|\mathbf{r}_p,f) = \frac{e^{ik|\mathbf{r}_p-\mathbf{r}_n|}}{4\pi|\mathbf{r}_p-\mathbf{r}_n|}. \quad (9)$$

This is justified because (1) multiple scattering is significant primarily between adjacent fish where the scattered field is propagated *directly* from one fish to the other without interaction with the waveguide boundaries, (2) the waveguide transmission loss is well approximated by the free space transmission loss at short ranges on the order of the water depth, as can be seen in Figs. 2.29 and 2.30 of Ref. 35, where the transmission losses shown for two 100 m deep Pekeris waveguides can be approximated as spherically spreading at ranges smaller than 100 m. The inter-fish propagation depends on the 3D positions of fish in a group, as well as the sound speed in the medium between the fish. Here, we assume this to be a constant of $c = 1482$ m/s, which is the mean sound speed at the fish group depth of 150 m (see Fig. 3 of Ref. 1).

B. Scattering properties of Atlantic herring

Here, we apply the theory described in Appendix B and Sec. II B to model the complex scatter function of an Atlantic herring individual and the corresponding result averaged over a group. Consider a group of $N = 10\,000$ fish centered at 150 m water depth, uniformly distributed over a 20 m thick depth layer with fork lengths derived from a Gaussian distribution of mean 24.2 cm and standard deviation 1.65 cm [Fig. 3(c)], consistent with the measured fork length distribution of trawl samples[1] collected during GOME06. The corresponding distribution of inferred swimbladder volumes for fish in the group is plotted in Fig. 3(d) with mean $V_m = 3.68$ ml and standard deviation $\sigma_V = 0.84$ ml, consistent with those inferred from the herring groups imaged on October 3, 2006, in Ref. 1 with estimated neutral buoyancy depth of 85 m. Note that even though the herring fork length distribution is modeled as Gaussian, the swimbladder volume distribution is not Gaussian and is asymmetric about the mean because the swimbladder volume depends nonlinearly on the fork length. It also depends on the depth location and the neutral buoyancy depth of each fish in the group.

The complex scattering amplitude, defined as the ratio of complex scatter function to wave number, $S(k)/k$, is plotted as a function of frequency for a herring of mean swimbladder volume 3.68 ml in Fig. 3(a). This fish has a resonance frequency near 1.6 kHz. Figure 3(b) illustrates the target strength spectrum as a function of frequency for the fish with mean swimbladder volume and for fish with swimbladder volumes both one standard deviation larger and smaller than the mean, as well as the ensemble-averaged target strength obtained by averaging the fish scattering cross-sections over the group, $TS = 10\log_{10}\overline{|S_p(k)/k|^2}$. A larger fish has a lower resonance frequency and a higher target strength at resonance. In Fig. 3(a), the imaginary part, $\Im\{S(k)/k\}$, peaks near resonance which indicates that both the scattering response from the fish group and the attenuation through the group increases near resonance. The imaging frequencies employed by the waveguide remote sensing system during GOME06 were in the sub-resonance range for the vast majority of herring imaged.

The roughly 1.6 kHz mean resonance frequency of the shoaling herring populations obtained in Ref. 1 from measurements made using the waveguide remote sensing system in the Gulf of Maine is comparable to published results of herring resonance frequency obtained with other local acoustic imaging systems.[5,36] As discussed in the last paragraph of page 115 in Ref. 1, "A wide distribution of swimbladder volumes and corresponding neutral buoyancy depths within any shoal is likely and could potentially unify the various existing data sets by superposition, with larger swimbladder volumes dominating at the lower end of the possible resonance spectrums and smaller volumes dominating the higher end. None of the systems used in the field so far, however, could test this since it would require acquisition of simultaneous data both well below and well above all contributing resonant frequencies." It should be noted that the data presented in Ref. 1 is the only data set existing for scattering from shoaling herring populations in the Gulf of Maine at frequencies below 1.5 kHz. The sources used in other studies[5,36,37] have sharp roll-offs in source level at frequencies below 2.5 kHz. The roughly 1.6 kHz mean resonance frequency measured with the waveguide remote sensing system in Ref. 1 was found to be consistent for the large herring shoals at roughly 150 m to 180 m water depth for all 10 days of observation in Fall 2006. This resonance was obtained by matching the low frequency roll-off in scattering from the large shoals which is the most robust method for estimating the resonance of a harmonic oscillator as discussed in Ref. 38 and shown in Sec. IV H. The waveguide remote sensing system used to measure fish target strength in Ref. 1 was also calibrated against scattering from deeply submerged BBN cylindrical air-filled targets during GOME06.[39]

IV. ILLUSTRATIVE EXAMPLES

Here, the theory described in Sec. II is applied to simulate the broadband matched filtered scattered field from groups of Atlantic herring imaged by the waveguide remote sensing system during GOME06. The effects of multiple scattering, attenuation due to scattering, and modal dispersion on fish population density imaging are investigated. The charting speed required to accurately localize a fish group in range from its time-dependent scattered field and the range resolution of the imaging system after matched filtering in the ocean waveguide are examined.

The modeled source waveform is a Tukey windowed linear frequency modulated pulse of 1 s duration and 50 Hz bandwidth with a center frequency f_c of either 415, 735, 950, or 1125 Hz, similar to those transmitted by the waveguide remote sensing system during GOME06. The waveform centered at 950 Hz is considered in the majority of examples illustrated here since the images formed from this waveform had the best cross-range resolution with significantly high fish scattered intensity to background reverberant intensity ratios and were used extensively for population density estimation in Refs. 1–3. The source and receiver arrays are centered at depths $z_0 = 65$ m and $z_r = 105$ m, respectively, to match typical imaging geometries of the waveguide remote sensing system employed in GOME06. The horizontal position of the source and receiver arrays are co-located in the examples presented here to simplify charting of scattered

returns in range, although a bistatic geometry was employed in GOME06. In all examples, the fish group is centered at 14.9 km horizontal range from the source and receiver arrays. The matched filtered returns in time are charted to horizontal range using $\rho = c_{\text{chart}}t/2$, where c_{chart} is the optimal charting speed determined in Sec. IV E. All results are normalized for a 0 dB re 1 μPa at 1 m source level. The bathymetric transect over which the signal propagates is provided in Sec. III A. The bottom is assumed to be sandy in all examples, unless otherwise specified. Roughly 100 independent broadband Monte-Carlo simulations are used to compute the scattered field statistics for each fish group discussed in this article, unless otherwise specified.

In all the examples to follow, we assume the cross-range resolution of the imaging system is equal to the cross-range extent of each fish group considered, and the main lobe is steered in the direction of the fish group so that we can approximate $\mathcal{B}(\phi_p) \approx 1$ for all fish in the group. Scattered returns from the fish group are compared to background reverberation derived from GOME06 data. The expected reverberation level *RL* at a given horizontal location $\boldsymbol{\rho}_p$ is estimated for each frequency band making use of the mean background scattering strength obtained from Fig. 5 of Ref. 1 and subtracting the broadband two-way transmission losses to horizontal location $\boldsymbol{\rho}_p$ from the source and receiver, and adding 10 $\log_{10} A_{\text{res}}(\boldsymbol{\rho}_p)$, where $A_{\text{res}}(\boldsymbol{\rho}_p)$ is the resolution footprint of the imaging system considered in the examples here.

For fish groups considered here, the maximum range and cross range extents are limited to 1 km and 100 m, respectively, because of computational constraints in modeling the scattered field moments numerically by Monte-Carlo simulation. The fish group sizes considered here are large compared to the wavelength of the imaging system, and similar in dimension to the small schools imaged in GOME06. For larger shoals imaged in GOME06, the results obtained here are still applicable to each resolution cell of the imaging system. This is because (1) multiple scattering is negligible, as we will show, for the vast majority of fish groups imaged, (2) even at imaging frequencies and fish volumetric densities where multiple scattering is significant, multiple scattering is important primarily between nearest neighbors spaced within several body lengths apart and negligible for fish with larger spatial separations. For the examples considered here, multiple scattering between neighbors located all 4π radian solid angle from an individual is included for the vast majority of fish, except for individuals near the cross-range periphery of each group where the multiple scattering is restricted to neighbors located within 2π radian solid angle. The multiply scattered fields from these latter individuals are expected to be negligibly small compared to the overall scattered level, given the large number of fish within each resolution cell of the imaging system.

A. Coherent and incoherent broadband matched filtered scattered intensities that include multiple scattering from a fish group compared to environmental reverberation

The coherent and incoherent broadband matched filtered fully scattered intensities from a group of Atlantic herring in the Gulf of Maine, which include multiple scattering, obtained from 100 independent broadband Monte-Carlo realizations are shown in Fig. 4(b) and 4(c). The imaging frequency band is centered at $f_c = 950$ Hz. The 3D spatial configurations that fish group adopt are derived from random realizations of a uniform probability distribution function (PDF) in depth and cross-range, and a non-uniform PDF in range shown in Fig. 4(a). The PDF in range is uniform in the middle, but with the front and back edges tapered with a half-Gaussian function. The simulated fish group has a total of $N = 10\,000$ individuals centered at $z_s = 150$ m depth with group extending $L_r = 100$ m in range, $L_{cr} = 100$ m in cross-range, and $L_z = 20$ m in depth, resulting in an average volumetric fish density of $N/(L_r\ L_{cr}\ L_z) = 0.05$ fish m^{-3} and an average areal fish density of $N/(L_r\ L_{cr}) = 1$ fish m^{-2}, matching typical densities found during GOME06 shown in Figs. 4D and 4E of Ref. 1.

The variance or incoherent intensity exceeds the squared mean or coherent intensity by about 20 dB. The incoherent intensity stands roughly 12 dB above background reverberation implying the fish group with areal density of 1 fish m^{-2} is highly detectable. For higher fish densities typically found in the shoal centers exceeding 10 fish m^{-2}, the fish scattered intensity to reverberation ratio will be proportionally higher, exceeding 20 dB.

For the given fish density, multiple scattering is found to be negligible for both the incoherent and coherent intensities. The first 4 orders of multiple scattering are included in the field, higher orders being insignificant. Differences

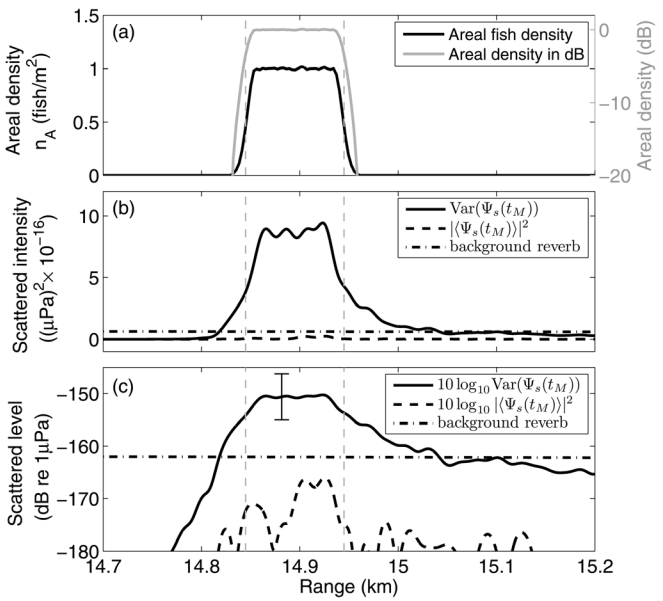

FIG. 4. (a) The areal density plotted as a function of range for a fish group in the Gulf of Maine environment with sand bottom. The vertical lines indicate the range where the fish areal density is half its maximum value. (b) The incoherent Var[$\Psi_s(t_M)$] and coherent $|\langle\Psi_s(t_M)\rangle|^2$ broadband matched filtered fully scattered intensities that include multiple scattering from the fish group imaged using the waveform centered at $f_c = 950$ Hz with 50 Hz bandwidth and 0 dB re 1 μPa at 1 m source level. The fish scattered intensities are compared to the expected background reverberation estimated from GOME06 data. (c) Identical to (b) but plotted in logarithmic scale. The error bar indicates the standard deviation of the broadband matched filtered fully scattered intensities from the fish group.

between the singly scattered level and the fully scattered level that includes multiple scattering are less than 0.1 dB over the entire extent of the fish group as shown in Fig. 5 and discussed in the next section.

A fully randomized PDF was used in this section to model the 3D spatial configuration of the fish group. In Sec. IV H and Sec. IV I, we show that for fish groups larger than the acoustic wavelength, the incoherent intensity dominating the fully scattered returns is independent of the specific 3D spatial configuration adopted by the group but is dependent on its areal and volumetric densities. For smaller fish groups on the order of the wavelength, we show the coherently scattered intensity dominates and is sensitive to the exact 3D spatial configuration adopted by the fish group.

B. Effects of multiple scattering and dependence on fish density and target strength

The single scattering assumption is often employed to estimate population density from scattered intensity in both waveguide remote sensing systems and conventional ultrasonic fisheries echosounders, since the scattered intensity is linearly related to population density when this assumption is valid.[1–4,12,28,40] When multiple scattering contributes to the full scattered intensity, however, the population density estimation may become non-linear. Here we examine the dependence of multiple scattering on herring target strength, which is a function of the imaging frequency, and population density.

Herring scatter functions and corresponding target strengths are highly dependent on imaging frequency as shown in Fig. 3. The effect of varying herring target strength by varying the imaging frequency band is investigated in Fig. 5. We consider broadband waveforms with the same four center frequencies as those transmitted by the vertical source array in GOME06. The parameters of the fish group and waveguide environment are identical to the example shown in Fig. 4. The scattered field levels from the fish group increase dramatically with target strength as the imaging frequency band increases toward resonance. Multiple scattering effects are only noticeable at the highest frequency band with $f_c = 1125$ Hz for the fish density considered. Even in this case, the differences between the singly scattered intensity levels and the fully scattered intensity levels that include multiple scattering are less than 0.5 dB.

The effects of multiple scattering are investigated with increasing fish densities in Fig. 6 for the $f_c = 950$ Hz band. The fish groups have identical dimensions $L_r = 50$ m, $L_{cr} = 50$ m, and $L_z = 20$ m, but contain (1) $N = 2500$, (2) $N = 10\,000$, and (3) $N = 40\,000$ individuals with fully randomized spatial configurations in each case. These examples correspond to fish volumetric densities of 0.05, 0.2, and 0.8 fish m^{-3} and areal densities of 1, 4, and 16 fish m^{-2}, respectively, as shown in Fig. 6(a). All other properties of the fish group and waveguide environment are identical to the example shown in Fig. 4. The variance or incoherent intensity increases roughly linearly with fish density, standing increasingly above background reverberation. The singly and fully scattered intensities are identical except when the fish areal density approaches and exceeds 16 fish m^{-2}. In this case, the fully scattered intensities differ from the singly scattered intensities by less than 0.5 dB. These differences also depend on attenuation as the field forward propagates through the fish group. The effect of attenuation in scattering is investigated in greater detail in the next section.

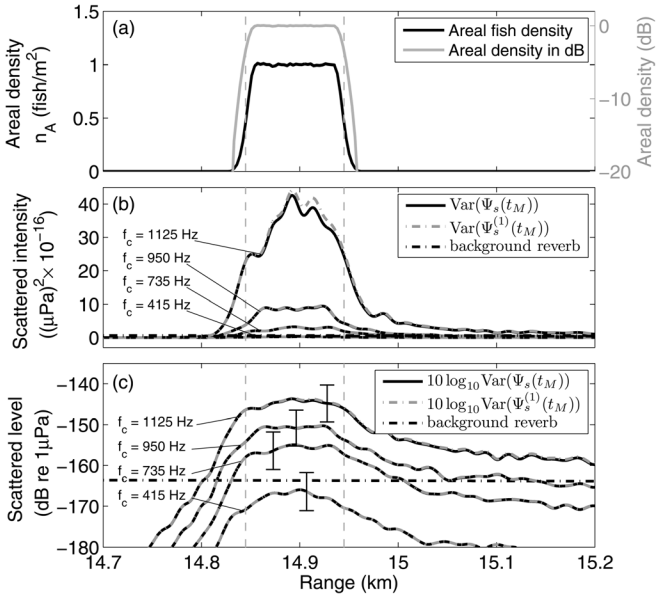

FIG. 5. Effect of varying the imaging frequency band on the incoherent matched filtered scattered returns from a fish group. (a) The areal density of the fish group. (b) The incoherent fully scattered intensity Var[$\Psi_s(t_M)$] that includes multiple scattering and singly scattered intensity Var [$\Psi_s^{(1)}(t_M)$] from the fish group are plotted as a function of the imaging frequency band. The expected background reverberant intensity estimated from GOME06 data is also plotted for comparison. The background reverberation varies by roughly 2 to 3 dB from the lowest to the highest frequency band and the average across the 4 bands is plotted here. (c) Identical to (b) but plotted in logarithmic scale. The error bars show the standard deviation of the broadband matched filtered fully scattered intensities from the fish group at various imaging frequency bands.

These examples validate the single scattering assumption employed in Refs. 1–3 to estimate herring areal population densities from their experimentally measured scattered intensities by the waveguide remote sensing system with frequency band centered at $f_c = 950$ Hz and below, since multiple scattering is negligibly small even at the highest areal/volumetric herring densities observed in GOME06. For herring areal population density imaging with frequency band centered at $f_c = 1125$ Hz, multiple scattering effects may matter at the shoal centers with very high fish densities as we illustrate in the next section.

C. Attenuation from scattering through a fish group and its dependence on swim-bladder resonance damping

The conditions under which multiple scattering becomes significant is often similar to that required for attenuation from forward scattering to become significant. When the volumetric density of the scatterers and their corresponding target strengths are high, multiple scattering leads to delayed returns that can enhance the overall scattered level over the range extent of the group. However, the close proximity of the scatterers to each other also imply that the forward

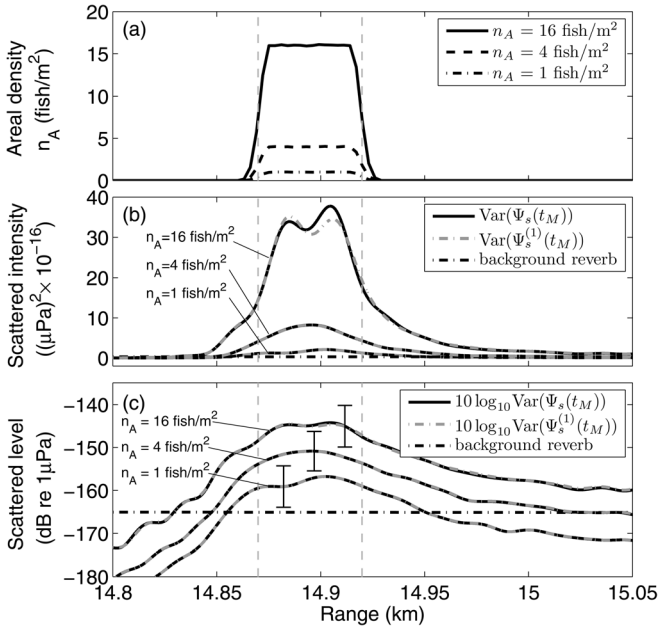

FIG. 6. Effect of varying the fish areal density on the broadband incoherent matched filtered scattered returns from a fish group imaged with frequency band centered at $f_c = 950$ Hz. (a) The areal fish densities of three distinct fish groups. (b) The incoherent fully Var[$\Psi_s(t_M)$] and singly Var [$\Psi_s^{(1)}(t_M)$] scattered intensities from the fish groups with imaging frequency band centered at 950 Hz are compared to background reverberation. (c) Identical to (b) but plotted in logarithmic scale. The error bars show the standard deviation of the broadband matched filtered fully scattered intensities from fish group with various fish areal densities.

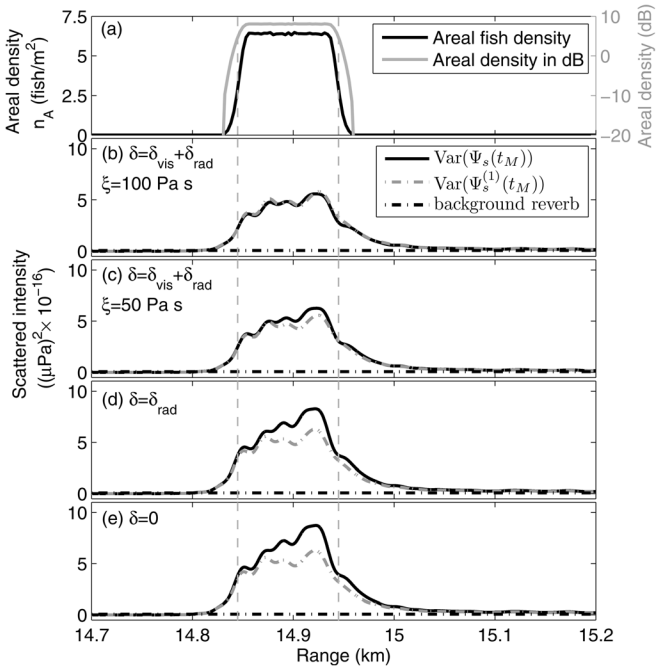

FIG. 7. Effect of varying fish swimbladder damping on the incoherent matched filtered scattered returns with imaging frequency band centered at 950 Hz. (a) The areal fish density of the fish group. (b)–(e) The incoherent fully Var[$\Psi_s(t_M)$] and singly Var[$\Psi_s^{(1)}(t_M)$] scattered intensities from the fish group are plotted as a function of fish damping coefficient, and compared to background reverberation.

scattered field from one scatterer can interfere destructively with the incident field at the location of another scatterer, as described by the extinction or forward scatter theorem.[14,16,41] This leads to shadowing and a corresponding reduction in the scattered intensity from the second scatterer, since the total field incident on it is reduced. This attenuation is dependent on the imaginary part of the forward scatter function of the scatterers and their spatial separations. Both multiple scattering and attenuation are cumulative over the range extent of the group and the effects are opposing.

Determining the attenuation from forward propagation through a fish group requires an accurate characterization of swimbladder resonance damping. The damping coefficient is not easily measured particularly for live *in situ* fish, since it depends on many factors and physical parameters of the swimbladder wall and surrounding fish flesh.[42] As discussed in Ref. 43, the Love model[44,45] may oversimplify the resonant damping by modeling the fish flesh as a viscous fluid.

Here we investigate the effect of varying the damping coefficients[43] on the scattered intensity from a group of herring in Figs. 7 and 8 with imaging frequency bands centered at $f_c = 950$ Hz and $f_c = 1125$ Hz, respectively. The fish group considered contains $N = 8000$ individuals with volumetric density of 0.64 fish m^{-3}, areal density of 6.4 fish m^{-2}, and dimensions $L_r = 100$ m, $L_{cr} = 12.5$ m, $L_z = 10$ m, as shown in Figs. 7(a) and 8(a). This group is elongated in range compared to its cross-range and depth dimensions to enhance the effects of multiple scattering and attenuation. All other properties of the fish group and waveguide environment are identical to the example shown in Fig. 4. Figures 7(b) and 7(c) and Figs. 8(b) and 8(c) include both viscous and radiation damping. These should be compared with the results in Figs. 7(d) and 8(d) where only radiation damping is included, and Figs. 7(e) and 8(e) with zero damping coefficient. When no damping is present [Figs. 7(e) and 8(e)] the scatter function is purely real and the fully scattered incoherent intensity that

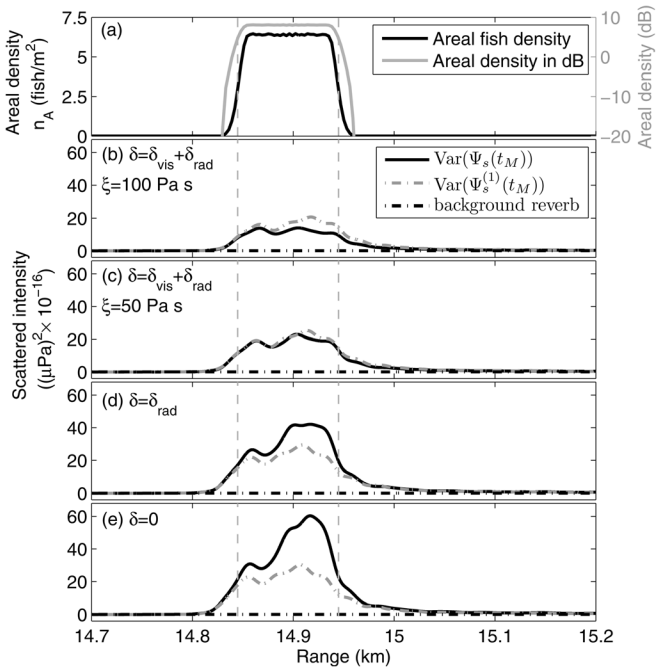

FIG. 8. Identical to Fig. 7 but for imaging frequency band centered at 1125 Hz.

includes multiple scattering increases cumulatively above the singly scattered intensity over the range extent of the group. When damping is included, attenuation through the group negates the effects of multiple scattering and the overall backscattered intensity level compared to the singly backscattered intensity level depends on the the amount of damping included in the model. The effects are more prominent when the imaging frequency band is centered at $f_c = 1125$ Hz as shown in Fig. 8.

The mean broadband incident intensity in the random waveguide, along with the mean total intensity forward propagated through the fish group are shown in Figs. 9(a) and 9(b) for the imaging frequency bands centered at 950 and 1125 Hz, respectively, where both intensities are averaged over the 10 m depth layer of the fish group. When damping is absent, the mean total forward propagated intensity is higher than the mean incident intensity because multiple scattering raises the overall level and the effect is cumulative over the range extent of the group. In the cases when damping is present, the total forward propagated intensities can fall below the incident intensity depending on the amount of damping included in the model. It should be noted that the incident intensity does not decay monotonically with range in Fig. 9 because of slight modal interference still present in the field even after averaging over 100 independent broadband Monte-Carlo realizations.

The analysis in this section indicates that both multiple scattering, and attenuation due to scattering are negligible in the long-range acoustic data at imaging frequency bands centered at 950 Hz and below and for the herring densities observed during GOME06. When the imaging frequency band is centered at 1125 Hz, the effects are non-negligible at the shoal centers and an accurate knowledge of swimbladder resonance damping is required to determine the amount of attenuation present in the data.

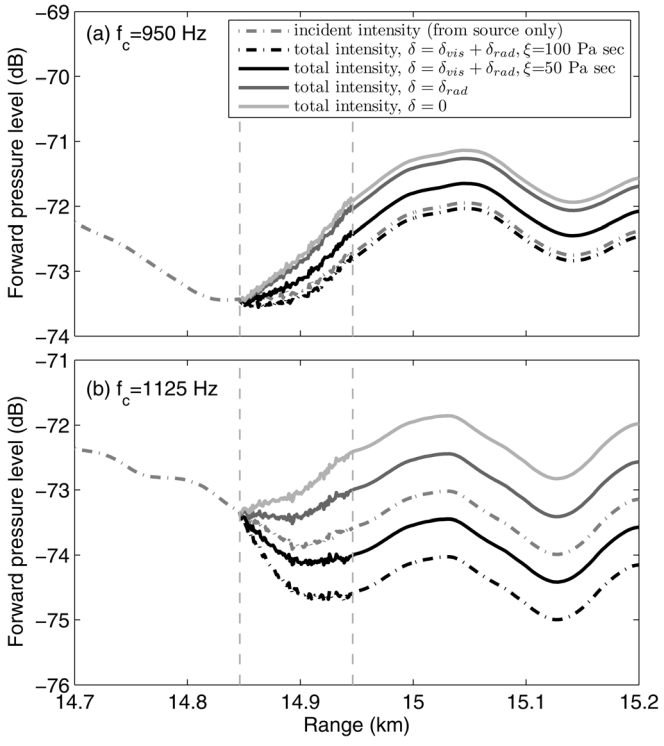

FIG. 9. The mean total acoustic intensity *forward* propagated through the fish group in Figs. 7 and 8 are plotted as a function of fish swimbladder damping for imaging frequency bands centered at (a) $f_c = 950$ Hz and (b) $f_c = 1125$ Hz. The broadband incident and forward propagated (which include multiple scattering from other fish in the group) intensities are averaged over the fish layer depth and over the 100 independent Monte-Carlo realizations.

D. Effect of modal dispersion

The incoherent intensity scattered from the fish group at the tail end of the distribution in Fig. 4 decays gradually as a function of range compared to the front end of the distribution. This is caused by modal dispersion, slowly propagating high-order modes that arrive later in time than the low order modes. The level of the dispersed returns are highly dependent on the waveguide and seafloor type. Compare the results in Fig. 4 for the sand waveguide to Fig. 10 for the silt waveguide. The properties of the fish group, imaging geometry, and all other properties of the waveguide are identical in these two examples, with the exception of the seafloor type. The silt seafloor has sound speed 1520 m/s, density 1.4 g/cm^3, and attenuation 0.3 dB/wavelength.

In the silt waveguide, the incoherent intensity scattered from fish at the tail end of the distribution decays more rapidly with range than in the sand waveguide and at a spatial rate approximately equal to that at the front end of the distribution. This is because the silt waveguide supports fewer number of propagating modes than the sand waveguide. The small contrast in sound speed between the water column and the seafloor allows only the very low order modes to propagate in a silt waveguide. For this reason, the effect of modal dispersion is minimized in the silt waveguide. The fewer number of propagating modes in the silt waveguide also implies that the total energy propagated through the waveguide is weaker. As a result, the scattered levels from the fish group and the background reverberation are both lower in the silt waveguide than in the sand waveguide. The

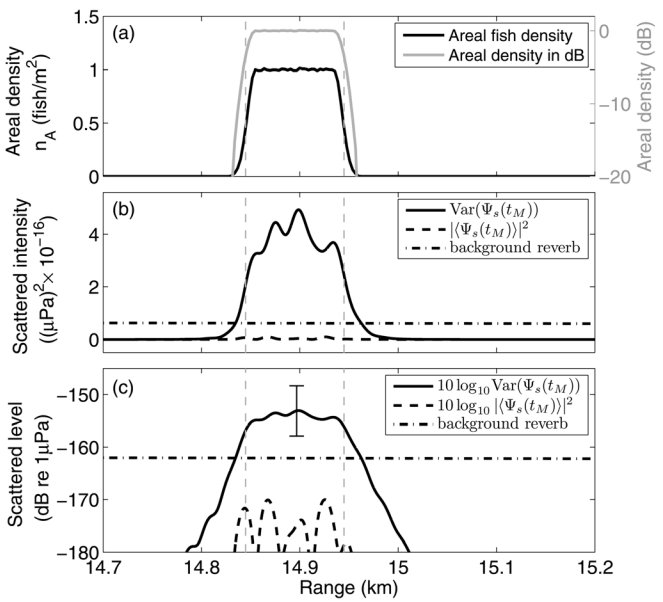

FIG. 10. Identical to Fig. 4 but for the silt waveguide.

background reverberation for the silt waveguide is obtained by subtracting 15 dB from the experimentally determined reverberation in the sand waveguide. This is because bottom reverberation modeling in Refs. 30 and 32 indicate that reverberation from the seafloor in the silt waveguide will be roughly 15 dB lower than in the sand waveguide.

E. Charting speed in the random range-dependent Gulf of Maine environment

Charting the time-dependent broadband matched filtered scattered intensity accurately in horizontal range for a target in a random ocean waveguide requires an optimal choice of the mean charting speed c_{chart}. In a waveguide imaging system, the scattered intensities from targets arriving at the same time instance at the receiver are charted onto an elliptical arc[6,46] in the horizontal plane with their respective azimuths determined via beamforming. The source and receiver arrays are located at the foci of the ellipse since the total horizontal path length from source to target $|\boldsymbol{\rho}_t - \boldsymbol{\rho}_0|$ and target to receiver $|\boldsymbol{\rho} - \boldsymbol{\rho}_t|$ satisfy[6] $|\boldsymbol{\rho}_t - \boldsymbol{\rho}_0| + |\boldsymbol{\rho} - \boldsymbol{\rho}_t| = c_{\text{chart}} t$. For the monostatic imaging scenario, since $\boldsymbol{\rho} = \boldsymbol{\rho}_0$, the range-time relationship simplifies to $|\boldsymbol{\rho} - \boldsymbol{\rho}_t| = c_{\text{chart}} t/2$.

Determining the optimal charting speed in a random range-dependent ocean waveguide can be challenging because sound speed is a function of depth, range, and time. Furthermore, the acoustic modes of the waveguide each propagate with a different group speed. Here, we determine the mean charting speed to be that which maximizes the modeled mean time-dependent broadband matched filtered scattered intensity at the true horizontal range span of the fish group.

The optimal mean charting speed is obtained when the variance or incoherent intensity integrated over the range extent of the group, $\int_{r_s - L_r/2}^{r_s + L_r/2} \text{Var}[\Psi_s(t)] dr$, is maximized, since there are no other scatterers present in the waveguide and the incoherent intensity is dominant. The mean charting speed in the sand waveguide for the example of Fig. 4 is found to be 1475 m/s with a standard deviation of 1.9 m/s. For the silt waveguide, the mean charting speed is 1474.4 m/s with a standard deviation of 1.1 m/s. For both waveguides, their respective mean charting speeds correspond roughly to the group speed of mode 1 in that waveguide. The charting accuracy is limited by the range resolution of the imaging system of roughly 15 m for the examples considered here. The estimated mean charting speed for all other examples are provided in Table I.

The charting speeds obtained here for actively localizing random scatterers in the random range-dependent ocean waveguide are approximately equal to the minimum of the mean water-column sound speed profile shown in Fig. 3 of Ref. 1. This result is consistent with that obtained in Ref. 26 for passive localization of a deterministic source in a range-independent ocean waveguide.

F. Fish areal population density estimation

Here, we show that the areal population density of fish groups can be readily estimated from their incoherently averaged broadband matched filtered scattered intensities when the single scattering assumption is valid. The areal population density n_A is estimated by correcting for (1) the broadband source level SL, (2) the broadband two-way transmission losses TTL_W obtained from waveguide Green's functions averaged over multiple realizations and over the depth extent of the fish layer, (3) the broadband target strength TS obtained from the mean scattering cross section of an individual fish, and (4) the resolution footprint A_{res} of the waveguide remote sensing system via,[1–4,12]

$$10\ \log_{10}\left\langle \overline{n_A(\boldsymbol{\rho}_p)} \right\rangle \approx L(\boldsymbol{\rho}_p) - SL(f_c) - TTL_W(\boldsymbol{\rho}_p, z_s, f_c) - TS(f_c) - 10\log_{10}\left[A_{\text{res}}(\boldsymbol{\rho}_p)\right], \quad (10)$$

where

$$L(\boldsymbol{\rho}_p, f_c) = 10\log_{10}\left\langle \left|\Psi(\boldsymbol{\rho}_p, f_c)\right|^2 \right\rangle \quad (11)$$

is the level of the measured or modeled incoherently averaged broadband matched filtered scattered intensity charted to horizontal range $\boldsymbol{\rho}_p$,

$$SL(f_c) = 10\log_{10}\left\langle \int_{f_c - B/2}^{f_c + B/2} |Q(f)|^2 df, \right\rangle \quad (12)$$

the $TTL_W(\boldsymbol{\rho}_p, z_s, f_c)$ is defined in Eq. (8),

$$TS(f_c) = 10\log_{10}\left\langle \frac{1}{E_0} \int_{f_c - B/2}^{f_c + B/2} |Q(f)|^2 |S(k)/k|^2 df \right\rangle, \quad (13)$$

and $A_{\text{res}}(\boldsymbol{\rho}_p) \approx \Delta\rho L_{cr}(\boldsymbol{\rho}_p)$, where $L_{cr}(\boldsymbol{\rho}_p)$ is the cross-range resolution, and $\Delta\rho = c_{\text{chart}}/2B$ is the range resolution after applying the matched filter. Reference 24 describes how the broadband transmission loss can be approximated using

TABLE I. Standard deviations, σ, of the broadband matched filtered scattered intensities from fish groups and corresponding estimated charting speeds, c_{chart}. The standard deviation of the estimated charting speed is roughly 1 to 2 m s^{-1}.

Figures	f_c (Hz)	B (Hz)	n_V (fish m^{-3})	SC[a]	Seafloor type	σ (dB)	c_{chart} (m s^{-1})
Fig. 4	950	50	0.05	random	sand	5.0	1475.0
Fig. 5	415	50	0.05	random	sand	5.5	1474.6
	735	50	0.05	random	sand	5.4	1475.6
	950	50	0.05	random	sand	5.0	1475.0
	1125	50	0.05	random	sand	4.9	1475.2
Fig. 6	950	50	0.05	random	sand	5.3	1473.6
	950	50	0.2	random	sand	5.4	1473.6
	950	50	0.8	random	sand	5.5	1473.6
Fig. 10	950	50	0.05	random	silt	5.3	1474.4
Fig. 11	950	50	0.05	random	sand	5.0	1475.0
	950	150	0.05	random	sand	3.6	1474.3
	950	50	0.05	random	silt	5.3	1474.4
	950	150	0.05	random	silt	4.5	1474.4
Fig. 12	950	50	0.025	random	sand	4.3	1474.3
Fig. 14	950	50	0.05	lattice	sand	5.0	1474.5
	950	50	0.05	random	sand	5.1	1474.3

[a]Three-dimensional spatial configuration of the simulated fish group.

the single frequency transmission loss as a function of range in a fluctuating waveguide by first spatial averaging the center frequency transmitted intensity and then transforming to log, $TTL_W(\boldsymbol{\rho}_p, z_s, f_c) \approx 10\log_{10}\{(4\pi)^2 \int_{z_s-D/2}^{z_s+D/2} \langle |G_W(\boldsymbol{\rho}_p, z_p|\mathbf{r}_0, f_c)|^2 |G_W(\mathbf{r}|\boldsymbol{\rho}_p, z_p, f_c)|^2 P(\boldsymbol{\rho}_p, z_p)\rangle dz_p\}$. This allows a rapid estimation of the fish areal population densities over wide areas for a single transmission and over multiple transmissions with varying source and receiver locations.

We consider two examples, the fish groups in Figs. 4 and 10 that extend only 6 resolution cells in range, and a much larger fish shoal that extends 60 resolution cells in range. The areal densities of the former fish groups in the sand and silt waveguides are estimated using Eq. (10) and are shown in Figs. 11(a) and 11(b), respectively. We consider two distinct frequency bandwidths for the source waveform centered at 950 Hz. When the imaging bandwidth is $B = 50$ Hz, the matched filter operation smooths over the edges of the distribution. This is because the corresponding matched filter resolution of 15 m is not sufficiently fine to resolve the edge of the fish distribution over range since the distribution decays rapidly from 1 to 0 fish m^{-2} over a 5 m range. By increasing the imaging bandwidth to $B = 150$ Hz, the edges of the distribution can be more accurately mapped[12] since the system has a finer range resolution of 5 m. For the fish groups in Fig. 11, the total population estimation error varies from 2% to 18% depending on the seafloor type and imaging bandwidth.

In contrast, a much larger fish group extending 1 km in range is modeled in Fig. 12 with imaging frequency centered at 950 Hz and $B = 50$ Hz. The fish group contains $N = 100\,000$ fish, has dimensions $L_r = 1000$ m, $L_{cr} = 100$ m, and $L_z = 40$ m, volumetric density of 0.025 fish m^{-3} and areal density of 1 fish m^{-2} as shown in Fig. 12(a). This fish group has a fully randomized 3D spatial configuration. All other properties of the fish group and waveguide environment are identical to the example shown in Fig. 4. Only the singly scattered field is calculated because multiple scattering is insignificant at this imaging frequency and volumetric density as shown in Sec. IV B. In addition, neglecting multiple scattering allows the numerical model to simulate much

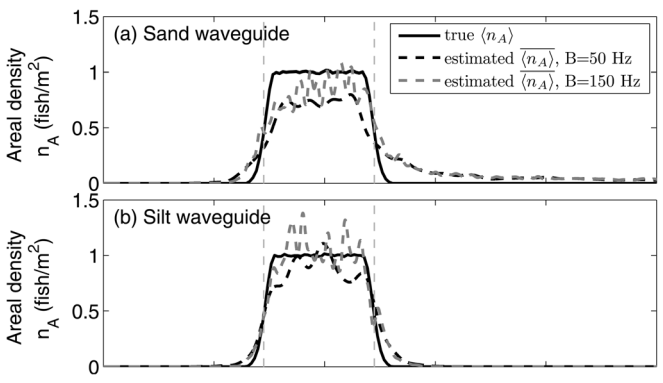

FIG. 11. (a) Estimating fish areal population densities from their incoherently averaged broadband matched filtered fully scattered intensities using Eq. (10) illustrated for the fish group in Fig. 4 in the sand waveguide as a function of imaging frequency bandwidth B with $f_c = 950$ Hz. (b) Identical to (a) but for the fish group in the silt waveguide shown in Fig. 10.

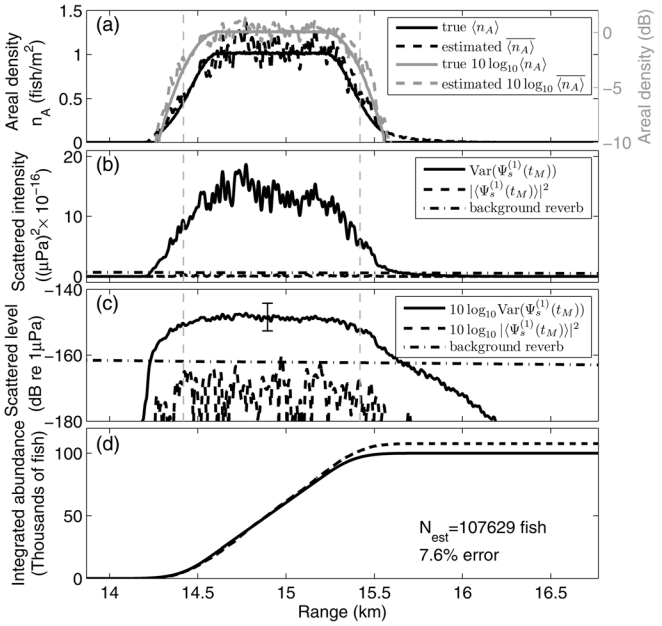

FIG. 12. Estimating fish areal population densities from their incoherently averaged broadband matched filtered scattered intensities illustrated for a much larger fish group. (a) True and estimated areal fish densities are plotted as a function of range. (b) The incoherent $\mathrm{Var}[\Psi_s^{(1)}(t_M)]$ and coherent $|\langle\Psi_s^{(1)}(t_M)\rangle|^2$ broadband matched filtered singly scattered intensities from the fish group imaged using the waveform centered at $f_c = 950$ Hz with 50 Hz bandwidth and 0 dB re 1 μPa source level are compared to background reverberation. (c) Identical to (b) but plotted in logarithmic scale. The error bar indicates the standard deviation of the broadband matched filtered singly scattered intensities from the fish group. (d) The true and estimated fish populations integrated as a function of range.

larger groups of fish because multiple scattering computations require an N^2 matrix multiplication, whereas single scattering requires only vectors of dimension N. The PDF in range for this group is uniform in the middle and tapered with half-Gaussian functions at the edges. The Gaussian edge region contains 20% of the total fish population in this example.

The estimated areal densities match the true densities on average over most of the group's extent except at the trailing edge of the distribution where the estimated densities are slightly higher due to modal dispersion. Figure 12(d) plots the cumulative true and estimated populations integrated over the range extent of the group. The integrated populations match fairly well throughout except at the trailing edge of the distribution. The total population estimation error is roughly 7.6%. Since the fish density decays gradually with range at the edges of this distribution, the 15 m range resolution after matched filtering is sufficiently fine to trace the edges, on average, for this example.

The examples in this section indicate that the range resolution of the imaging system after matched filtering the broadband scattered waveform in the random range-dependent ocean waveguide is approximately equal to that obtained in free-space, $\Delta\rho \approx c_{\mathrm{chart}}/2B$. This is because the total fish population estimated from the scattered intensities using Eq. (10) are approximately equal to the true population when the range resolution is defined as in free-space. Dispersion in the multi-modal waveguide has negligible effect on the matched filter resolution for waveforms with bandwidths up to 150

Hz and center frequencies in the range of 300 to 1200 Hz investigated here.

G. Standard deviation of the broadband matched filtered scattered intensities from the fish group

The standard deviation of the scattered returns must be accurately known in order to determine error bounds in population density estimation and to determine sample sizes necessary for reducing uncertainty.[47] The standard deviations of the broadband matched filtered fully scattered intensities within each resolution cell of the imaging system, determined from 100 independent Monte-Carlo realizations for each of the fish groups considered in this section are tabulated in Table I. The standard deviations are also indicated by error bars in the respective figures. They are approximately 5 dB for most of the fish groups considered here, implying that the received broadband matched filtered scattered fields can be approximated as statistically saturated with phases that are almost fully randomized.[23] This result is consistent with the measured intensity standard deviations determined from instantaneous images of the waveguide remote sensing system.[1–4] There, a 6-sample averaging, from averaging adjacent pixels in range and three consecutive instantaneous wide-area images over time, was employed to reduce the standard deviations in the scattered intensity images to less than 1.5 dB.[1–4] This standard deviation for each pixel is small compared to the dynamic range of scattered intensity levels spanned by the fish groups.

When the incoherent intensity dominates, the standard deviation of the scattered returns are independent of the spatial configuration adopted by the large fish group considered in Sec. IV I (see Table I). The standard deviations of the scattered levels from the fish group considered here are larger than the standard deviations of the broadband two-way transmission losses in the ocean waveguide (see Sec. III A) since the former incorporates additional sources of randomness, such as individual fish spatial locations and scatter functions.

H. Coherent multiple scattering effects such as resonance shift and sub- and super-resonance local maxima

Multiple scattering from a dense fish group can lead to effects such as a shift in the resonance frequency for the group from that of a single fish, and sub- and super-resonance local maxima. These phenomena have been predicted and explained in Refs. 17, 18, and 20. Here, we show that these effects are only significant for fish groups that are very dense and small, on the order of the acoustic wavelength, where the coherently scattered intensity is significant. Fish groups observed in the Gulf of Maine were many orders of magnitude larger and had lower volumetric densities. The incoherent intensity dominated the scattered returns so that the coherent multiple scattering effects are negligible as shown here.

Two distinct fish groups are considered, one with dimensions much larger than the acoustic wavelength and the other with dimensions on the order of the wavelength. The large herring group contains 7831 individuals with volumetric density $n_V = 0.05$ fish m^{-3} distributed over a volume, as shown in Fig. 1(b), with axes dimensions given by $L_x = 100$ m, $L_y = 100$ m, and $L_z = 20$, while the smaller group contains 240 individuals distributed over a similar volume but with axes dimensions given by $L_x = 2$ m, $L_y = 2$ m and $L_z = 2$ m, with a volumetric density $n_V = 37.5$ fish m^{-3} that is many orders of magnitude denser than the herring groups typically observed during GOME06. Both groups are centered at $z_s = 150$ m depth and are imaged by a monostatic direct-path imaging system. We consider two distinct 3D spatial configurations for both the large and small fish group, the fully randomized and the partially random lattice configurations discussed in Sec. II B.

The analysis in this section follow the approach outlined in Sec. II C, except that 100 independent Monte-Carlo realizations are used here to estimate the statistical moments of the scattered intensities, including multiple scattering, at each frequency. The coherent, incoherent, total and estimated school target strength spectra calculated using Eqs. (2), (3), (4), and (5) are plotted in Figs. 13(a) and 13(b) for the large and small fish groups, respectively, as a function of the fish group spatial configuration. For the large fish group, the incoherent intensity dominates the total scattered returns. The total school target strength spectrum is well approximated by the estimated school target strength spectrum assuming single scattering. For this case, the total target strength spectrum is independent of the specific 3D spatial configuration adopted by the fish group.

In contrast, for the small fish group, the coherently scattered intensity is significant, causing a shift in the resonance frequency of the group. It also leads to sub- and super-resonance local maxima as shown in Fig. 13(b). In this case, the specific spectrum of the coherent, incoherent and total school target strengths are dependent on the 3D spatial configuration

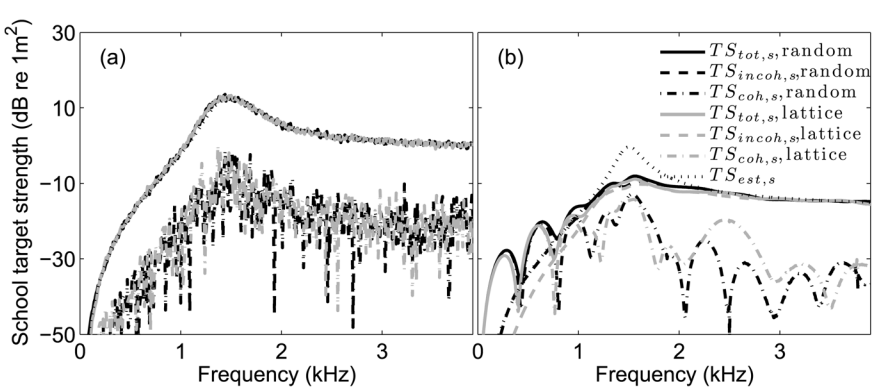

FIG. 13. Effect of the 3D spatial configuration on the time harmonic fully scattered field moments, including multiple scattering, as a function of frequency for a monostatic direct-path imaging system examined for (a) a large herring group containing 7831 individuals and (b) a small herring group containing 240 individuals. The coherent, incoherent, total and estimated *school* target strength spectra calculated via Eqs. (2)–(5), respectively, are compared as a function of the fish group configuration.

adopted by the fish group. The total school target strength is roughly 2 to 3 dB larger when fish in the group follow the fully random spatial configuration rather than the partially random lattice configuration.

The analysis in this section has important implications for the measurement of resonance frequency of fish groups. For instance, a local direct path acoustic system that has high spatial resolution in depth typically images significantly fewer number of fish, 10 to a few hundred individuals, within its resolution footprint. Such a system may make errors in estimating the resonance frequency of a fish group especially if its operating frequency does not span the mean resonance frequency range of the fish group. This is because the system may measure the local super- or sub-resonance maxima resulting from coherent scattering interactions between fish, as shown in Figs. 2 and 13(b). This is less of an issue for the waveguide remote sensing system since there are significantly many more fish, typically several thousand or more, within each resolution footprint so that scattering is dominated by the incoherent intensity that peaks at just one frequency, the mean resonance frequency for the fish group.

I. Effect of fish group 3D spatial configuration

Here we examine the effect of the 3D spatial configuration of a fish group on the statistical moments of its broadband matched filtered fully scattered intensities that include multiple scattering in a random ocean waveguide. We consider a herring group containing 7831 individuals with volumetric density $n_V = 0.05$ fish m^{-3} distributed over a volume, as shown in Fig. 1(b), with axes dimensions $L_x = 100$ m, $L_y = 100$ m, and $L_z = 20$ m. This herring group is located at range $r_s = 14.9$ km from the source and receiver arrays at depth $z_s = 150$ m and is imaged with a broadband waveform of 50 Hz bandwidth centered at $f_c = 950$ Hz in the ocean waveguide with sand seafloor.

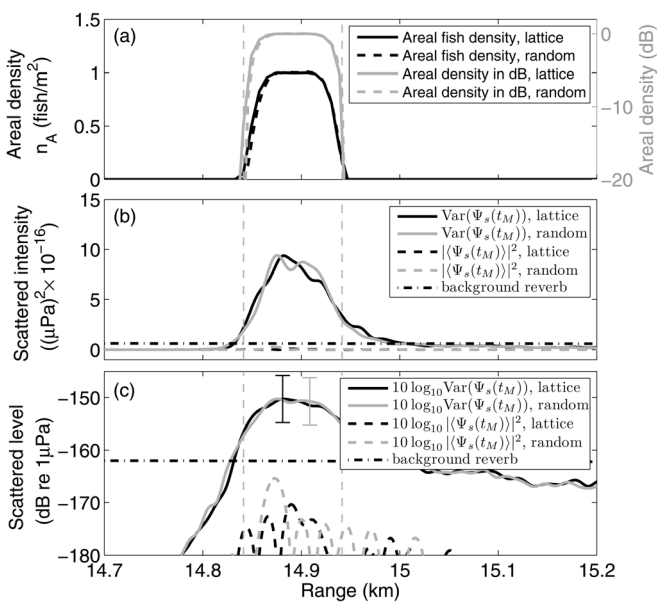

FIG. 14. Effect of the 3D spatial configuration of a fish group on the statistical moments of its broadband matched filtered fully scattered intensities. (a) The areal fish densities in the two configurations. (b) The incoherent Var[$\Psi_s(t_M)$] and coherent $|\langle\Psi_s(t_M)\rangle|^2$ broadband matched filtered fully scattered intensities that include multiple scattering from the fish groups imaged using the waveform centered at $f_c = 950$ Hz with 50 Hz bandwidth and 0 dB re 1 μPa at 1 m source level. The fish scattered intensities are compared to the expected background reverberant intensities estimated from GOME06 data. (c) Identical to (b) but plotted in logarithmic scale.

In Fig. 14, we consider two distinct 3D spatial configurations for the fish group, the fully randomized and the partially random lattice configurations discussed in Sec. II B. The range extent of this fish group is much larger than the acoustic wavelength and the scattered returns are dominated by the incoherent intensity. The dominant incoherent broadband matched filtered fully scattered intensities that include multiple scattering are approximately equal for fish in the two spatial configurations and local differences are negligible small compared to the dynamic range of intensity fluctuations indicated by the error bars in Fig. 14(c). For this example, the specific 3D spatial configuration adopted by the fish group has negligible effect on the mean scattered intensity, which is consistent with the results shown in Fig. 13(a) for the same fish group, but imaged by a monostatic direct-path system in an iso-speed lossless non-random environment.

When the fish group dimension is on the order of the acoustic wavelength, the scattered intensities depend on the specific 3D spatial configuration adopted by the fish group as discussed in Sec. IV H.

V. CONCLUSION

A numerical model has been developed to determine the statistical moments of the broadband matched filtered scattered field including multiple scattering from a random 3D spatial distribution of random scatterers in a random range-dependent ocean waveguide by Monte-Carlo simulation. The model can be applied to analyze bistatic scattering from a scatterer group in any direction including the forward. When combined with the incident field, the model can accurately characterize attenuation in forward propagation through a group. The model is applied to examine population density imaging of shoaling Atlantic herring using a waveguide remote sensing system in the 300 to 1200 Hz frequency range in the Gulf of Maine during GOME06. A herring swimbladder is modeled as damped air-filled prolate spheroid surrounded by viscous flesh using a complex scatter function.

Analysis with the model indicate that (1) the incoherent intensity dominated the scattered returns from large herring groups imaged during GOME06 and effects such as resonant shift and sub- and super-resonance local maxima are negligible or absent, (2) the single scattering assumption is valid for inferring herring areal population densities from their scattered intensities over the imaging frequency range and observed herring densities during GOME06, (3) waveguide dispersion had negligible effect on herring shoal population estimation, (4) the standard deviations of the instantaneous broadband matched filtered scattered intensities from the fish groups are roughly 5 dB indicating that the scattered fields are fully saturated and that the standard deviations can be reduced by stationary averaging, (5) the charting speed for accurately localizing targets in range from their time-dependent scattered fields after matched filtering in a random

waveguide is approximately equal to the average group speed of the lowest order mode, and (6) the imaging system's range resolution in the waveguide is approximately equal to its resolution in free space where it is inversely proportional to the system bandwidth.

ACKNOWLEDGMENTS

We thank Nicholas C. Makris for providing the initial motivation for this work. This research was funded by the Office of Naval Research, the National Oceanographic Partnership Program and the Alfred P. Sloan Foundation with administrative support from Bernard M. Gordon Center for Subsurface Sensing and Imaging Systems. This research is a contribution to the Census of Marine Life.

APPENDIX A: MODEL FOR THE BROADBAND MATCHED FILTERED FULLY SCATTERED FIELD FROM A GIVEN DISTRIBUTION OF SCATTERERS INCLUDING MULTIPLE SCATTERING

Here we describe the theoretical model used to calculate the broadband matched filtered fully scattered field from a given 3D spatial distribution of distinct scatterers that includes multiple scattering. The formulation follows the approach of Ref. 12. The imaging geometry, source, receiver and fish coordinates are described in Sec. II A.

Given a group containing N scatterers, the time-harmonic total scattered field received at frequency f,

$$\Phi_s(\mathbf{r},f) = \sum_{p=1}^{N} A(\phi_p)\mathcal{B}(\phi_p)\Phi_s(\mathbf{r},p,f), \tag{A1}$$

is a sum of the fully scattered fields from each of the scatterers within the group, where $\mathcal{A}(\phi_p)$ and $\mathcal{B}(\phi_p)$ are the beampatterns of the imaging system source and receiver arrays respectively weighting the contribution from the pth scatterer. Here $\mathcal{A}(\phi_p)$ can be approximated as 1 because the vertical source array of the waveguide remote sensing system has an azimuthally symmetric beampattern. $\Phi_s(\mathbf{r}, p, f)$ is the fully scattered field[21,22] from the pth scatterer, formulated here as a sum of the singly scattered field, $\Phi_s^{(1)}(\mathbf{r},p,f)$, and the multiply scattered field, $\Phi_s^{(MS)}(\mathbf{r},p,f)$,

$$\begin{aligned}\Phi_s(\mathbf{r},p,f) &= \Phi_s^{(1)}(\mathbf{r},p,f) + \Phi_s^{(MS)}(\mathbf{r},p,f)\\ &= Q(f)G(\mathbf{r}_p|\mathbf{r}_0,f)G(\mathbf{r}|\mathbf{r}_p,f)\frac{S_p(\Omega_i,\Omega_s,k)}{k}\\ &\quad + \sum_{q=1,q\neq p}^{N}\Phi_s(\mathbf{r}_p,q,f)G(\mathbf{r}|\mathbf{r}_p,f)\frac{S_p(\Omega_{qp},\Omega_s,k)}{k},\end{aligned} \tag{A2}$$

where G is the medium's Green's function, $S_p(\Omega_i, \Omega_s, k)$ is the scatter function[16,48] for the pth scatterer which depends on wave number $k = 2\pi f/c$ and the direction of the incident and scattered plane waves,[15,16,48] Ω_i and Ω_s, respectively. The scatter function can be used to model general scatterers of arbitrary size compared to the wavelength.

Upon substituting Eq. (A2) into Eq. (A1), the time harmonic fully scattered field becomes

$$\begin{aligned}\Phi_s(\mathbf{r},f) &= \Phi_s^{(1)}(\mathbf{r},f) + \Phi_s^{(MS)}(\mathbf{r},f)\\ &= \sum_{p=1}^{N}\mathcal{B}(\phi_p)\Phi_s^{(1)}(\mathbf{r},p,f) + \sum_{p=1}^{N}\mathcal{B}(\phi_p)\Phi_s^{(MS)}(\mathbf{r},p,f),\end{aligned} \tag{A3}$$

where $\Phi_s^{(1)}(\mathbf{r},f)$ is the time harmonic singly scattered field, and $\Phi_s^{(MS)}(\mathbf{r},f)$ is the time harmonic multiply scattered field from all N scatterers received at frequency f.

In Eq. (A2), the multiply scattered field $\Phi_s^{(MS)}(\mathbf{r},p,f)$ at $\mathbf{r}$ from the pth scatterer depends on the sum of the acoustic fields first scattered from all other $N-1$ scatterers and incident on the pth scatterer, with each term given by $\Phi_s(\mathbf{r}_p,q,f)$. In order to solve Eq. (A2) for all N scatterers, we must find the scattered field incident on each scatterer from all other $N-1$ scatterers. This is expressed as

$$\begin{aligned}\Phi_s(\mathbf{r}_n,p,f) &= Q(f)G(\mathbf{r}_p|\mathbf{r}_0,f)G(\mathbf{r}_n|\mathbf{r}_p,f)\frac{S_p(\Omega_i,\Omega_{pn},k)}{k}\\ &\quad + \sum_{q=1,q\neq p}^{N}\Phi_s(\mathbf{r}_p,q,f)G(\mathbf{r}_n|\mathbf{r}_p,f)\frac{S_p(\Omega_{qp},\Omega_{pn},k)}{k},\end{aligned} \tag{A4}$$

where n and p are variables indicating that the field incident on n is scattered from p, $\mathbf{\Omega}_{qp}$ is the incident angle onto p scattered from q and $\mathbf{\Omega}_{pn}$ is the scattered angle from p scattered onto n. Equation (A4) has a similar form as Eq. (A2) in terms of both singly and multiply scattered fields. Equations (A2) and (A4) expressed in terms of the object's plane wave scatter function are valid[16,49] in the far-field of each scatterer, where r_p, $|\mathbf{r}_0 - \mathbf{r}_p|$, and $|\mathbf{r}_n - \mathbf{r}_p|$ are all greater than a_p^2/λ, where a_p is the largest dimension of the pth scatterer.

The matched filter[9–11] is a normalized replica of the original transmitted waveform,

$$H(f|t_M) = \frac{1}{\sqrt{E_0}}Q^*(f)e^{i2\pi f t_M}, \tag{A5}$$

where t_M is the time delay of the matched filter and $E_0 = \int |Q(f)|^2 df$ is the source energy. Applying Fourier synthesis, the time-dependent matched filtered fully scattered field from the scatterer group, including multiple scattering, can be expressed as

$$\Psi_s(t_M) = \int_B \Phi_s(\mathbf{r},f)H(f|t_M)e^{-i2\pi f t}df \tag{A6}$$

an integral involving Eq. (A1) over the signal bandwidth.

Substituting Eq. (A3) into Eq. (A6), the time dependent matched filtered fully scattered field can be decomposed into,

$$\begin{aligned}\Psi_s(t_M) &= \Psi_s^{(1)}(t_M) + \Psi_s^{(MS)}(t_M)\\ &= \int_B \Phi_s^{(1)}(\mathbf{r},f)H(f|t_M)e^{-i2\pi f t}df\\ &\quad + \int_B \Phi_s^{(MS)}(\mathbf{r},f)H(f|t_M)e^{-i2\pi f t}df,\end{aligned} \tag{A7}$$

a sum of the time-dependent matched filtered singly scattered field, $\Psi_s^{(1)}(t_M)$, and the time-dependent matched filtered multiply scattered field, $\Psi_s^{(MS)}(t_M)$.

APPENDIX B: MODELING FISH SWIMBLADDER AS A DAMPED AIR-FILLED PROLATE SPHEROID

There are several models[44,50,51] that describe the scattering properties of a swimbladder near resonance. Here we model a fish swimbladder near resonance as a damped air-filled oscillator[17,18,20,43,52] and take into account the prolate spheroidal shape of the swimbladder through a correction term to the resonance frequency developed by Weston,[51] as well as the damping from viscosity of the surrounding fish flesh modeled by Love.[44] This model approximates the swimbladder as a viscous heat-conducting shell enclosing an air cavity with surface tension at the inner surface[44,45] that leads to a damped resonance behavior. Given a fish of swimbladder volume V_z (m^3) at depth z (m), its *complex* scatter function is,[52]

$$S(k) = \frac{\left(\frac{f_0^2}{f^2} - 1\right) k\bar{a}}{\left(\frac{f_0^2}{f^2} - 1\right)^2 + \delta^2} + i\frac{\delta k\bar{a}}{\left(\frac{f_0^2}{f^2} - 1\right)^2 + \delta^2}, \tag{B1}$$

where f_0 is the resonance frequency (Hz) and $\bar{a} = \left(\frac{3}{4\pi} V_z\right)^{1/3}$ is the equivalent radius (m) of the swimbladder. The dimensionless damping coefficient,

$$\delta = \delta_{\text{rad}} + \delta_{\text{vis}} = k\bar{a} + \frac{\xi_f}{\pi \bar{a}^2 f \rho_f}, \tag{B2}$$

is a sum of the radiation damping δ_{rad} and the viscous damping δ_{vis}. The contribution from thermal damping is assumed to be negligible.[44] In Eq. (B2), the physical properties of fish, such as the fish flesh density ρ_f (kg m^{-3}) and viscosity ξ_f (Pa s) are usually empirically determined. For instance, the viscosity and flesh density for Atlantic herring have been experimentally found to be $\xi_f = 50$ Pa s (Ref. 45) and $\rho_f = 1071\ \text{kg m}^{-3}$ (Ref. 53), respectively. The resonance frequency of a prolate spheroid shaped swimbladder is given by

$$f_0 = \frac{\zeta}{2\pi\bar{a}} \sqrt{\frac{3\gamma P_z}{\rho_f}}, \tag{B3}$$

where $\gamma = 1.40$ is the ratio of specific heats of air and water, and P_z is the ambient pressure at depth z. The correction term for the spheroidal shaped swimbladder,[51] ζ, is given by

$$\zeta = \frac{\sqrt{2}(1-\epsilon^2)^{1/4}}{\epsilon^{1/3}} \left\{ \ln\left[\frac{1+\sqrt{1-\epsilon^2}}{1-\sqrt{1-\epsilon^2}}\right] \right\}^{-1/2}, \tag{B4}$$

where eccentricity ϵ is the ratio of semi-minor to semi-major axis of the prolate spheroid. For the herring groups modeled in this paper, $0.1 < \epsilon < 0.2$.[1]

The swimbladder volume V_z at depth z of an individual from a given fish species may be estimated using length and weight measurements of trawl samples of the species, and the fact that for most swimbladder-bearing fish, the air-filled swimbladder typically comprises roughly 4% to 5% of fish body volume V_b (m^3) at neutral buoyancy depth z_{nb} (m).[54] For a fish of fork length L (cm), its body volume can be estimated from

$$V_b = \frac{W}{\rho_f} = \frac{1}{\rho_f} pL^q, \tag{B5}$$

where p and q are regression parameters[55] empirically determined from length L and weight W measurements of trawl samples. The swimbladder volume at any depth z can then be determined using Boyle's law,

$$P_{nb}V_{nb} = P_z V_z, \tag{B6}$$

where (P_{nb}, V_{nb}) are the ambient pressure and swimbladder volume at neutral buoyancy depth z_{nb}, and (P_z, V_z) are the ambient pressure and volume at any depth z.

Applying the extinction theorem[14,16] and substituting Eq. (B2) into Eq. (B1), the total extinction cross section σ_{ext} of fish swimbladder that accounts for energy removed from the forward direction can be expressed as a sum of the scattering σ_{sca} and absorption σ_{abs} cross sections,[43]

$$\begin{aligned}\sigma_{\text{ext}} &= \frac{4\pi}{k^2} \Im\{S_f(k)\} = \sigma_{\text{sca}} + \sigma_{\text{abs}} \\ &= \frac{4\pi}{k^2} \frac{\delta k\bar{a}}{\left(\frac{f_0^2}{f^2} - 1\right)^2 + \delta^2} \\ &= \frac{4\pi\bar{a}^2}{\left(\frac{f_0^2}{f^2} - 1\right)^2 + \delta^2} + \frac{4\pi\bar{a}^2(\delta_{\text{vis}}/\delta_{\text{rad}})}{\left(\frac{f_0^2}{f^2} - 1\right)^2 + \delta^2}\end{aligned} \tag{B7}$$

where $S_f(k)$ is the scatter function in forward direction. Note that the scattering cross section σ_{sca} is consistent with that of Love's model.[44,45]

In summary, given the measured fish length and depth distributions, the empirically determined length-volume regression Eq. (B5), and assuming the prolate spheroidal swimbladder has a major axis that is a constant percentage of the total fish length [usually 26% to 33% (Ref. 36 and 56)] and only changes in the minor-axis of the swimbladder contributes to volume change because of physiological constraints in fish anatomy,[36,56–58] the complex scatter function of a given fish at frequency f in Eq. (B1) then only depends on a single parameter, the swimbladder volume V_z at depth z or equivalently the neutral buoyancy depth.

[1] Z. Gong, M. Andrews, S. Jagannathan, R. Patel, J. M. Jech, N. C. Makris, and P. Ratilal, "Low-frequency target strength and abundance of shoaling Atlantic herring (Clupea Harengus) in the Gulf of Maine during the Ocean Acoustic Waveguide Remote Sensing 2006 Experiment," J. Acoust. Soc. Am. **127**, 104–123 (2010).

[2] N. C. Makris, P. Ratilal, S. Jagannathan, Z. Gong, M. Andrews, I. Bertsatos, O. R. Godo, R. W. Nero, and J. M. Jech, "Critical population density triggers rapid formation of vast oceanic fish shoals," Science **323**, 1734–1737 (2009).

[3] S. Jagannathan, D. Symonds, I. Bersatos, T. Chen, H. Nia, A. D. Jain, M. Andrews, Z. Gong, R. Nero, L. Ngor, M. Jech, O. Godoe, S. Lee,

P. Ratilal, and N. Makris, "Ocean acoustic waveguide remote sensing (OAWRS) of marine ecosystems," Mar. Ecol. Prog. Ser. **395**, 137–160 (2009).
[4]N. C. Makris, P. Ratilal, D. T. Symonds, S. Jagannathan, S. Lee, and R. W. Nero, "Fish population and behavior revealed by instantaneous continental shelf-scale imaging," Science **311**, 660–663 (2006).
[5]R. C. Gauss, J. M. Fialkowski, E. L. Kunz, R. Menis, T. K. Stanton, C. J. Sellers, and J. M. Jech, "Clutter variability due to fish aggregations: mid-frequency measurements in the Gulf of Maine," in *Proceedings of the 3rd International Conference and Exhibition on Underwater Acoustic Measurements: Technologies and Results*, edited by J. S. Papadakis and L. Bjorno (Nafplion, Peloponnese, Greece, 2009), pp. 459–466.
[6]N. C. Makris, L. Z. Avelino, and R. Menis, "Deterministic reverberation from ocean ridges," J. Acoust. Soc. Am. **97**, 3547–3574 (1995).
[7]G. D. Tyler, "The emergence of low-frequency active acoustics as a critical antisubmarine war fare technology," Johns Hopkins APL Tech. Dig. **13**, 145–159 (1992).
[8]P. Ratilal, Y. Lai, D. T. Symonds, L. A. Ruhlmann, J. R. Preston, E. K. Scheer, M. T. Garr, C. W. Holland, J. A. Goff, and N. C. Makris, "Long range acoustic imaging of the continental shelf environment: The Acoustic Clutter Reconnaissance Experiment 2001," J. Acoust. Soc. Am. **117**, 1977–1998 (2005).
[9]S. Stergiopoulos, *Advanced Signal Processing Handbook: Theory and Implementation for Radar, Sonar, and Medical Imaging Real-Time Systems* (CRC Press, Boca Raton, FL, 2001), Chaps. 6 and 11.
[10]G. L. Turin, "An introduction to matched filters," IEEE Trans. Inf. Theory. **IT-6**, 311–329 (1960).
[11]A. W. Rihaczek, *Principles of High-Resolution Radar* (Artech House, Boston, 1996), Chaps. 3 and 4.
[12]M. Andrews, Z. Gong, and P. Ratilal, "High resolution population density imaging of random scatterers with the matched filtered scattered field variance," J. Acoust. Soc. Am. **126**, 1057–1068 (2009).
[13]P. Ratilal and N. C. Makris, "Mean and covariance of the forward field propagated through a stratified ocean waveguide with three-dimensional random inhomogeneities," J. Acoust. Soc. Am. **118**, 3532–3559 (2005).
[14]H. C. van de Hulst, *Light Scattering by Small Particles* (Dover, New York, 1957), Chaps. 1, 4, and 18.
[15]L. Tsang, J. A. Kong, and K.-H. Ding, *Scattering of Electromagnetic Waves: Theories and Applications* (John Wiley, New York, 2000), Chaps. 6 and 7.
[16]M. Born and E. Wolf, *Principles of Optics* (Cambridge University Press, Cambridge, 1980), Chap. 13.
[17]R. W. Nero, C. Feuillade, C. H. Thompson, and R. H. Love, "Near-resonance scattering from arrays of artificial fish swimbladders," J. Acoust. Soc. Am. **121**, 132–143 (2007).
[18]T. Hahn, "Low frequency sound scattering from spherical assemblages of bubbles using effective medium theory," J. Acoust. Soc. Am. **122**, 3252–3267 (2007).
[19]T. Stanton, "Multiple-scattering with applications to fish echo-processing," J. Acoust. Soc. Am. **73**, 1164–1169 (1983).
[20]C. Feuillade, R. W. Nero, and R. H. Love, "A low-frequency acoustic scattering model for small schools of fish," J. Acoust. Soc. Am. **99**, 196–208 (1996).
[21]L. L. Foldy, "The multiple scattering of waves," Phys. Rev. **67**, 107–119 (1944).
[22]Z. Ye and A. Alvarez, "Acoustic localization in bubbly liquid media," Phys. Rev. Lett. **80**, 3503–3506 (1998).
[23]N. C. Makris, "The effect of saturated transmission scintillation on ocean acoustic intensity measurements," J. Acoust. Soc. Am. **100**, 769–783 (1996).
[24]M. Andrews, T. Chen, and P. Ratilal, "Empirical dependence of acoustic transmission scintillation statistics on bandwidth, frequency, and range in New Jersey continental shelf," J. Acoust. Soc. Am. **125**, 111–124 (2009).
[25]R. Headrick, J. F. Lynch, J. Kemp, A. Newhall, K. von der Heydt, J. R. Apel, M. Badiey, C.-S. Chiu, S. Finette, M. H. Orr, B. H. Pasewark, A. Turgut, S. Wolf, and D. Tielbuerger, "Acoustic normal-mode fluctuation statistics in the 1995 SWARM internal wave scattering experiment," J. Acoust. Soc. Am. **107**, 201–220 (2000).
[26]G. Bar-Yehoshua, "Quantifying the effect of dispersion in continental shelf sound propagation," Ph.D. thesis, Massachusetts Institute of Technology, Cambridge, MA, 2002.
[27]Y. Lai, "Acoustic scattering from stationary and moving targets in shallow water environments - with application of humpback whale detection and localization," Ph.D. thesis, Massachusetts Institute of Technology, Cambridge, MA, 2004.
[28]D. N. MacLennan and E. J. Simmonds, *Fisheries Acoustics*, 2nd ed. (Chapman and Hall, London, 1992), pp. 61–62 and 177–182.
[29]M. D. Collins, "Generalization of the split-step pade," J. Acoust. Soc. Am. **96**, 382–385 (1994).
[30]N. C. Makris and P. Ratilal, "A unified model for reverberation and submerged object scattering in a stratified ocean waveguide," J. Acoust. Soc. Am. **109**, 909–941 (2009).
[31]F. Ingenito, "Scattering from an object in a stratified medium," J. Acoust. Soc. Am. **82**, 2051–2059 (1987).
[32]P. Ratilal, "Remote sensing of submerged objects and geomorphology in continental shelf waters with acoustic waveguide scattering," Ph.D. thesis, Massachusetts Institute of Technology, Cambridge, MA, 2002.
[33]J. R. Apel, M. Badiey, C.-S. Chiu, S. Finette, R. Headrick, J. Kemp, J. F. Lynch, A. Newhall, M. H. Orr, B. H. Pasewark, D. Tielbuerger, A. Turgut, K. von der Heydt, and S. Wolf, "An overview of the 1995 SWARM shallow-water internal wave acoustic scattering experiment," IEEE J. Ocean. Eng. **22**, 465–500 (1997).
[34]L. D. McGinnis and R. M. Ottis, "Compressional velocities from multichannel refraction arrivals on Georges's Bank-northwest Atlantic Ocean," Geophysics **44**, 1022–1032 (1979).
[35]F. B. Jensen, W. A. Kuperman, M. B. Porter, and H. Schmidt, *Computational Ocean Acoustics* (Springer-Verlag, New York, 1993), pp. 120–126.
[36]R. W. Nero, C. H. Thompson, and J. M. Jech, "In situ acoustic estimates of the swimbladder volume of Atlantic herring (*Clupea harengus*)," ICES J. Mar. Sci. **61**, 323–337 (2004).
[37]T. Stanton, D. Chu, J. M. Jech, and J. D. Irish, "New broadband methods for resonance classification and high-resolution imagery of fish with swimbladders using a modified commercial broadband echosounder," ICES J. Mar. Sci. **67**, 365–378 (2010).
[38]A. P. French, *Vibrations and Waves*, MIT Introductory Physics Series, 41–76 (CRC Press, Boca Raton, FL, 1971).
[39]S. Jagannathan, "Sensing animal group behavior and bio-clutter in the ocean over continental shelf scales," Ph.D. thesis, Massachusetts Institute of Technology, Cambridge, MA, 2011.
[40]K. G. Foote, "Linearity of fisheries acoustics, with addition theorems," J. Acoust. Soc. Am. **73**, 1932–1940 (1983).
[41]P. Ratilal and N. C. Makris, "Extinction theorem for object scattering in a stratified medium," J. Acoust. Soc. Am. **110**, 2924–2945 (2001).
[42]C. Feuillade and R. W. Nero, "A viscous-elastic swimbladder model for describing enhanced- frequency resonance scattering from fish," J. Acoust. Soc. Am. **103**, 3245–3255 (1998).
[43]T. Chen, "Mean, variance, and temporal coherence of the 3d acoustic field forward propagated through random inhomogeneities in continental-shelf and deep ocean waveguides," Ph.D. thesis, Massachusetts Institute of Technology, Cambridge, MA, 2009.
[44]R. H. Love, "Resonant acoustic scattering by swimbladder-bearing fish," J. Acoust. Soc. Am. **64**, 571–580 (1978).
[45]R. H. Love, "A comparison of volume scattering strength data with model calculations based on quasisynoptically collected fishery data," J. Acoust. Soc. Am. **94**, 2255–2268 (1993).
[46]N. C. Makris, C. S. Chia, and L. T. Fialkowski, "The bi-azimuthal scattering distribution of an abyssal hill," J. Acoust. Soc. Am. **106**, 2491–2512 (1999).
[47]N. C. Makris, "Parameter resolution bounds that depend on sample size," J. Acoust. Soc. Am. **99**, 2851–2861 (1996).
[48]J. Bowman, T. Senior, and P. Uslenghi, *Electromagnetic and Acoustic Scattering by Simple Shapes*, 1–768 (North-Holland, Amsterdam, 1969).
[49]P. Ratilal, Y. Lai, and N. C. Makris, "Validity of the sonar equation and babinet's principle for scattering in a stratified medium," J. Acoust. Soc. Am. **112**, 1797–1816 (2002).
[50]I. B. Andreeva, "Scattering of sound by air bladders of fish in deep sound scattering ocean layers," Sov. Phys. Acoust. **10**, 17–20 (1964).
[51]D. E. Weston, "Sound propagation in the presence of bladder fish," in *Underwater Acoustics*, edited by V. M. Albers (Plenum Press, New York 1967), Vol. 2, pp. 55–88.
[52]T. G. Leighton, *The Acoustic Bubble* (Academic, London, 1994), pp. 298–301.
[53]V. M. Brawn, "Buoyancy of Atlantic and Pacific herring," J. Fish Res. Board Can. **26**, 2077–2091 (1969).
[54]F. R. Harden Jones and N. B. Marshall, "The structure and functions of the teleostean swimbladder," Biol. Rev. **28**, 16–83 (1953).
[55]S. E. Wigley, H. M. McBride, and N. J. McHugh, "Length-weight relationships for 74 fish species collected during NEFSC research vessel

bottom trawl surveys, 1992–99," Technical Report, NMFS, Woods Hole Lab., Woods Hole, MA, 2003.
[56]N. Gorska and E. Ona, "Modelling the effect of swimbladder compression on the acoustic backscattering from herring at normal or near-normal dorsal incidences," ICES J. Mar. Sci. **60**, 1381–1391 (2003).
[57]J. H. S. Blaxter and R. S. Batty, "The herring swimbladder as a gas reservoir for the acoustico-lateralis system," J. Mar. Biol. Assoc. U.K. **59**, 1–10 (1979).
[58]E. Ona, "Physiological factors causing natural variations in acoustic target strength of fish," J. Mar. Biol. Assoc. U.K. **70**, 107–127 (1990).